

Random Finite Set Theory and Optimal Control of Large Collaborative Swarms

Bryce Doerr*

University of Minnesota, Minneapolis, MN, 55455

Richard Linares†

Massachusetts Institute of Technology, Cambridge, MA, 02139

Pingping Zhu ‡ and Silvia Ferrari §

Cornell University, Ithaca, NY, 14853

Controlling large swarms of robotic agents has many challenges including, but not limited to, computational complexity due to the number of agents, uncertainty in the functionality of each agent in the swarm, and uncertainty in the swarm’s configuration. This work generalizes the swarm state using Random Finite Set (RFS) theory and solves the control problem using Model Predictive Control (MPC) to overcome the aforementioned challenges. Computationally efficient solutions are obtained via the Iterative Linear Quadratic Regulator (ILQR). Information divergence is used to define the distance between the swarm RFS and the desired swarm configuration. Then, a stochastic optimal control problem is formulated using a modified L_2^2 distance. Simulation results using MPC and ILQR show that swarm intensities converge to a target destination, and the RFS control formulation can vary in the number of target destinations. ILQR also provides a more computationally efficient solution to the RFS swarm problem when compared to the MPC solution. Lastly, the RFS control solution is applied to a spacecraft relative motion problem showing the viability for this real-world scenario.

I. INTRODUCTION

Control of large robotic networks or swarms is currently an area of great interest in controls research. These robotic groups are usually tiny robots with limited actuators that do specific tasks in the formation. For example, the group can use its combined effort to grasp or move in the environment [1]. Specifically, in space system applications, swarm control of satellites and rovers can be used for exploration of asteroids and other celestial bodies of interest [2]. In military applications, swarms of UAVs can be used for border patrol, search and rescue, surveillance, communications relaying, and mapping of hostile territory [3]. In reviewing these applications, swarm control of large groups of swarming agents

*Ph.D. Student, Department of Aerospace Engineering and Mechanics. Email: doerr024@umn.edu, AIAA Student Member.

†Charles Stark Draper Assistant Professor, Department of Aeronautics and Astronautics. Email: linaresr@mit.edu, Senior AIAA Member.

‡Research Associate, Department of Mechanical and Aerospace Engineering. Email: pingping.zhu@cornell.edu, AIAA Member.

§Professor, Department of Mechanical and Aerospace Engineering. Email: ferrari@cornell.edu, AIAA Member.

is required.

A key challenge involved with controlling swarms is the increase in computational complexity with increasing number of agents within the swarm [4]. As the state vector size increases (increase in dimension) for each additional agent added to the swarm, the computational complexity increases for the vector. Thus, for swarms of a thousand agents, it can take many hours to meet the control objectives using traditional approaches. Rubenstein observed that it took 10 hours for 1024 Kilobots to move into the desired formation [4]. These results show that the controller computational time as a function of the number of agents in the swarm is an important problem to consider.

Another challenge to consider is the uncertainty of each agent within the system [5]. Swarm systems that involve low-cost individual agents are not expected to function properly together during the period of control due to uncertainties in each agent. This behavior of each agent within the system cannot be accurately described without explicitly analyzing and modeling all uncertainty. It is difficult to compute heuristically, and it may be computationally expensive to incorporate. Even if the uncertainty is correctly described, there may be times the model is not valid during the swarm operation. With all these factors, it becomes increasingly difficult to accurately control low-cost swarms while considering the uncertainty of each low-cost agent.

Transmission of information in swarms is an area of concern, especially for low-cost swarms [5]. Every agent in the swarm may have complete measurement data on its system, but it may possess limited knowledge of the other agents in the swarm. If the other agents have contradictory goals compared to the first agent, the first agent will not be able to know the motive of the other agents as it goes through its routine, thus causing complications to the overall control objective. Thus, each agent may not know the overall state completely. To mitigate the information limitation, information structure constraints are imposed to achieve simplicity in the control strategies. Unfortunately, adding information constraints may lead to more complex modeling and analysis. For example, in swarm UAV control, aerial surveillance, tracking, and collision avoidance are all control objectives the swarm UAV may want to do [3]. These objectives rely on more robust sensors. Depending on the individual UAV's size, the swarm agent is limited hardware-wise on what information can be transmitted between agents. Thus, adding information constraints might be a necessary task to meet the control objectives.

Changing how the swarm state is represented and how its behavior is modeled in space and time has been shown to alleviate the computational complexity of control methods and solutions[6–10]. Previously, the swarm/potential model using the random finite set (RFS) formalism was used to describe the temporal evolution of the probabilistic description of the robot swarm to promote decentralized coordination [11]. By using a measure-value recursion of the RFS formalism for the agents of the swarm, the dynamics of the swarm in time can be determined with computational efficiency.

Several control techniques have been implemented on swarms to date. In centralized control, one agent in the swarm is the designated controller and manages the execution of other agents in the swarm [12]. Thus, it oversees the

other agents' system processes. This type of control is the easiest to implement on a swarm of robots, and it solves the problem of controlling the swarm to the desired state. Unfortunately, this type of control suffers from two main problems. As the number of agents of the swarm increases, the computational workload becomes more difficult. This is especially difficult when the swarm robots are low-cost robotic agents. Another issue that arises is that centralized control is not robust against failures of other agents within the swarm [13]. Since swarm robots on a level of a thousand agents are low-cost units, communication, actuation, and sensing are performed with less reliability. Thus, centralized control may not be a viable option for these systems.

Probabilistic swarm guidance has also been used to enable the swarm to converge to target distributions [14]. Probabilistic swarm guidance controls a swarm density distribution through distributed control so that each agent determines its own trajectory while the swarm converges to the target distribution. Distributed control is defined as reformulating a control problem as a set of interdependent subproblems and solving these subproblems [5]. Probabilistic swarm guidance solves issues that involve controlling an increasing number of individual agents which is computationally complex by controlling the swarm density distribution of the agents. Using optimal transport, convergence is achieved faster than a homogeneous Markov chain approach and the cost function is minimized [14, 15, 17]. Another method is the use of the inhomogeneous Markov chain [18, 19]. In this approach, the agents move in a decentralized fashion which is like the homogeneous Markov chain, but the algorithm allows communication with other agents to reach and settle at the target destination. These algorithms are robust to external disturbances since the algorithms themselves use the swarm density distribution.

Velocity field generation for swarm control is a non-optimal decentralized control method for swarms that synthesizes smooth velocity fields as a function of time and position [20]. With a designated target distribution, the swarm follows the velocity field using the heat equation to convergence by using local agent position information to estimate its local density. The advantage of this method is that the agents facilitate collision avoidance and move in a smoother manner than previous Markov chain approaches [15]. Unfortunately, the use of the heat equation diffuses the agents in a locally uniform manner to the target density. Therefore, this is a non-optimal method of controlling the swarm to a target distribution.

A distributed optimal control method was also used previously to control multi-agent systems by modeling the agents as Gaussian mixtures and using an integral cost function that is optimized to the advection equation (a partial differential equation that contains the dynamical constraint) [6–8]. The control laws themselves were determined using potential functions that attract the agent distributions to the desired state and repels the distribution from obstacles [16]. By minimizing the objective function based on distributions using the necessary conditions of optimality, the optimal control law was found using the potential function. The distributed optimal control method was expanded to use the Kullback-Leibler divergence metric using distributions in the objective function for the use of path planning [9]. This provides a discovery to a whole class of divergence measures of distributions that can provide converging optimal

control solutions to multi-agent systems.

Model predictive control (MPC) has been heavily studied for nonlinear systems and for applications including spacecraft maneuvering and attitude control [21–23]. Decentralized MPC has also been studied for thousands of low-cost spacecraft with limited capabilities [24]. This MPC method computes the control input by solving a finite horizon problem. This allows it to optimize the current time step while taking the future time steps into account. Therefore, it can use future events to make control decisions in the present. The benefits of this solution are that it decentralizes the computation and communication required for the swarm system. Thus, swarms of more than a thousand units can be controlled without being computationally expensive. Also, model predictive control decreases the run time of the convex programming and allows the algorithm to include constraints on each swarm agent. By using a decentralized configuration approach, any measurement and process uncertainties in the trajectories are accounted for within the algorithm. Thus, this provides robustness for the swarm while pushing the initial swarm to its desired state.

Another decentralized approach to controlling swarms is using sequential convex programming [25]. Sequential convex programming uses multiple iterations to maintain the accuracy of the convex approximations of the constraints which create more efficient trajectories. Uncertainties in the trajectories are accounted for when the algorithm is tuned. Using sequential convex programming in combination with MPC in real time provides the robustness for the swarm while pushing the agents to the designated targets. Morgan also used sequential convex programming to do target assignment (mapping of agents to targets) and trajectory generation for varying swarm sizes through time [26]. This method is viable for swarms, but through RFS control, target assignment is not necessary.

Although these approaches provide a method to control swarm agents, RFS control for large swarms provides computational performance for control of low-cost agents [27]. Their MPC solution minimizes the nonquadratic objective function based on the RFS formalism through optimization which is accurate but computationally slow. In this work, an RFS control problem using MPC and ILQR is presented to show the viability of ILQR compared to MPC. ILQR approximates a quadratic objective function, and iterates to determine a good solution. Therefore, ILQR provides a sub-optimal solution compared to MPC, but ILQR provides less complexity and lighter computational load than the MPC counterpart.

The objectives of the paper are to form the control background using RFS theory and to control swarming agents using MPC and ILQR in combination with behavioral distribution control. Through the RFS optimal control method, swarm intensities can converge to target destinations, repel each other, and vary in swarm size or target destinations. By using an ILQR solution, a quadratic approximation of the objective function is determined and minimized which decreases the computational complexity of minimizing the objective function compared to the MPC solution. Then, the RFS control method is applied to a physical spacecraft relative motion swarm problem with perfect and imperfect information. The Gaussian mixture probability hypothesis filter (GM-PHD filter) is used to provide estimates for RFS control which allows for the control of large spacecraft swarms.

II. Random Finite Set Control Problem Formulation

The framework to control swarming agents is to set up multiple-agent filtering problem using RFS theory [29, 30]. To formulate the multiple-agent filter problem, the single-agent filtering problem is discussed.

A. Single-Agent Filtering

When estimating the dynamical system for a single agent, it is usually assumed that the state space follows a Markov process with a transition density,

$$f_{k|k-1}(\mathbf{x}_k | \mathbf{x}_{k-1}), \quad (1)$$

to move discretely from the previous state \mathbf{x}_{k-1} to the next state at \mathbf{x}_k . Note that \mathbf{x}_k is for a single agent. For generality, the dynamical system is partially observed as a likelihood function given by

$$g_k(\mathbf{z}_k | \mathbf{x}_k), \quad (2)$$

where the likelihood function is a probability density of observing the system by obtaining measurements, \mathbf{z}_k . By using the observation information from $\mathbf{z}_{1:k} = (\mathbf{z}_1, \dots, \mathbf{z}_k)$, the posterior density estimate at a time k is determined using the Bayesian recursion given by

$$p_{k|k-1}(\mathbf{x}_k | \mathbf{z}_{1:k-1}) = \int f_{k|k-1}(\mathbf{x}_k | \mathbf{x}_{k-1}) p_{k-1}(\mathbf{x}_{k-1} | \mathbf{z}_{1:k-1}) d\mathbf{x}_{k-1}, \quad (3a)$$

$$p_k(\mathbf{x}_k | \mathbf{z}_{1:k}) = \frac{g_k(\mathbf{z}_k | \mathbf{x}_k) p_{k|k-1}(\mathbf{x}_k | \mathbf{z}_{1:k-1})}{\int g_k(\mathbf{z}_k | \mathbf{x}_k) p_{k|k-1}(\mathbf{x}_k | \mathbf{z}_{1:k-1}) d\mathbf{x}_k}. \quad (3b)$$

The posterior density contains the measurement update, and the estimate for this single-agent system can be found using a minimum mean squared error method.

B. RFS Formulation

The multi-agent problem considers the Bayesian recursion through a RFS formulation with discrete-time dynamics [30]. This theory addresses the decentralized formulation for each agent in the formation. Each agent has the challenge of estimating its local formation configuration and designing a decentralized control policy to achieve some local configuration. It is assumed that each agent within the swarm is identical and using unique identifiers on each agent is unnecessary. Using RFS theory, the number of agents and their states is determined from measurements. The agents in the field may die, survive and move into then next state through dynamics, or appear by spawning or birthing. The number of agents in the field is denoted by $N_{\text{total}}(t)$ and may be randomly varying at each time-step by the union of the birth ($\Gamma_k : \emptyset \rightarrow \{\mathbf{x}_{i,k}, \mathbf{x}_{i+1,k}, \dots, \mathbf{x}_{N_{\text{birth},k}}\}$), spawn ($B_{k|k-1}(\zeta) : \mathbf{x}_{i,k-1} \rightarrow \{\mathbf{x}_{i,k}, \mathbf{x}_{i+1,k}, \dots, \mathbf{x}_{N_{\text{spawn},k}}\}$), and surviving ($S_{k|k-1}(\zeta) : \mathbf{x}_{i,k-1} \rightarrow \mathbf{x}_{i,k}$) agents. Death is denoted by $D_k(\zeta) : \mathbf{x}_{i,k-1} \rightarrow \emptyset$. Note that $\mathbf{x}_{i,k}$ is for the i th

swarm agent's state. This is described by a RFS, X_k , given by

$$X_k = \left[\bigcup_{\zeta \in X_{k-1}} S_{k|k-1}(\zeta) \right] \cup \left[\bigcup_{\zeta \in X_{k-1}} B_{k|k-1}(\zeta) \right] \cup \Gamma_k. \quad (4)$$

$X_k = \{\mathbf{x}_{1,k}, \mathbf{x}_{2,k}, \dots, \mathbf{x}_{N_{total(k),k}}\}$ denotes a realization of the RFS distribution for agents. The individual RFS in Eq. (4) are assumed to be independent from each other. For example, any births that occur at any time-step are independent from any surviving agents. At any time, k , the RFS probability density function can be written as

$$p(X_k = \{\mathbf{x}_{1,k}, \mathbf{x}_{2,k}, \dots, \mathbf{x}_{n,k}\}) = p(|X_k| = n)p(\{\mathbf{x}_{1,k}, \mathbf{x}_{2,k}, \dots, \mathbf{x}_{n,k}\} \mid |X_k| = n). \quad (5)$$

For a generalized observation process, the agents are either detected ($\Theta_k(\mathbf{x}_k) : \mathbf{x}_{i,k} \rightarrow \mathbf{y}_{i,k}$), or undetected ($F_k(\mathbf{x}_k) : \mathbf{x}_{i,k} \rightarrow \emptyset$). Clutter or false alarms ($K_k : \emptyset \rightarrow \{\mathbf{y}_{1,k}, \mathbf{y}_{2,k}, \dots, \mathbf{y}_{N_{clutter,k}}\}$), defined as measurements that do not belong to any agents, are also present in the set of observations. Note that $\mathbf{y}_{i,k}$ is for the i th swarm agent's measurement. Therefore, RFS of measurements are described by

$$Z_k = K_k \cup \left[\bigcup_{\mathbf{x}_k \in X_k} \Theta_k(\mathbf{x}_k) \right], \quad (6)$$

where the origins of each measurement are not known and unique identifiers are not necessary. Again, the individual RFS in Eq. (6) are independent of each other, so measurements and clutter are obtained independently from each other. Single-agent filtering cannot be applied because measurements determined cannot be associated with which agent generated the measurement. By using the RFS formulation, measurements can be associated to individual agents in the swarm.

On a similar note, the control sequence is also defined by a RFS in the form $U_k = \{\mathbf{u}_{1,k}, \mathbf{u}_{2,k}, \dots, \mathbf{u}_{N_{total(k),k}}\}$ and a RFS probability density given by

$$p(U_k = \{\mathbf{u}_{1,k}, \mathbf{u}_{2,k}, \dots, \mathbf{u}_{n,k}\}) = p(|U_k| = n)p(\{\mathbf{u}_{1,k}, \mathbf{u}_{2,k}, \dots, \mathbf{u}_{n,k}\} \mid |U_k| = n), \quad (7)$$

since the number of the agents in the field to be controlled is also varying.

The random finite set formulation of describing multi-agent states and observations can be described very similarly to Eq. (1) and (2), but the RFS states (X_k) and observations (Z_k) are used instead. To determine the multi-agent posterior density, a multi-agent Bayes recursion is used given by

$$p_{k|k-1}(X_k | Z_{1:k-1}) = \int f_{k|k-1}(X_k | X_{k-1}) p_{k-1}(X_{k-1} | Z_{1:k-1}) \mu_s(dX_{k-1}), \quad (8a)$$

$$p_k(X_k|Z_{1:k}) = \frac{g_k(Z_k|X_k) p_{k|k-1}(X_k|Z_{1:k-1})}{\int g_k(Z_k|X_k) p_{k|k-1}(X_k|Z_{1:k-1}) \mu_s(dX_k)}, \quad (8b)$$

where μ_s is a reference measure on some function $F(X)$. The recursion is computationally expensive due to multiple integrals, but solutions have been found for a small number of targets using sequential Monte Carlo [28]. Fortunately, a PHD filter approximation provides computational tractability for a larger number of agents.

C. Probability Hypothesis Density (PHD) Filter

Instead of propagating the multi-agent posterior density through a multi-agent Bayes recursion, the Probability Hypothesis Density (PHD) filter propagates the posterior intensity function. The nonnegative intensity function, $v(\mathbf{x})$, is a first-order statistical moment of the RFS state that represents the probability of finding an agent in a region of state space S . The expected number of agents in the region S is the integral of the intensity function given by

$$E(|X \cap S|) = \int |X \cap S| P(dX) = \int_S v(\mathbf{x}) d\mathbf{x}, \quad (9)$$

where the expectation represents a RFS X intersecting a region S with a probability distribution P dependent on X . This gives the total mass or the expected number of agents of RFS X in a region S . The local maximum in intensity $v(\mathbf{x})$ show the highest concentration of expected number of agents which can be used to determine an estimate for the agents in X at a time-step.

Poisson RFS are fully characterized by their intensities. By assuming the RFS X is Poisson of the form $p(|X| = n)$ and $p(\{\mathbf{x}_1, \mathbf{x}_2, \dots, \mathbf{x}_n\} | |X| = n)$, approximate solutions can be determined by the PHD filter. Propagation of the PHD can be determined if the agents are assumed to be independent and identically distributed with the cardinality of the agent set that is Poisson distributed [30]. Clutter and birth RFS are assumed to be Poisson RFS. It is noted that the assumptions made by the PHD filter are strong assumptions for swarming robotics. However, this is a good starting point for an initial proof-of-concept study. The PHD recursion for a general intensity function, $v_t(\mathbf{x})$, is given by

$$\bar{v}_t(\mathbf{x}) = b(\mathbf{x}) + \int p_s(\zeta) f(\mathbf{x}|\zeta) v(\zeta) d\zeta + \int \beta(\mathbf{x}|\zeta) v(\zeta) d\zeta, \quad (10)$$

where $b(\mathbf{x})$, $p_s(\zeta)$, and $\beta(\mathbf{x}|\zeta)$ are the agents' birth, survival, and spawn intensity, $f(\mathbf{x}|\zeta)$ is the target motion model, and ζ is the previous state respectively [30]. The bar on $\bar{v}_t(\mathbf{x})$ denotes that the PHD has been time-updated. For the measurement update, the equation is given by

$$v_t(\mathbf{x}) = (1 - p_d(\mathbf{x})) \bar{v}_t(\mathbf{x}) + \sum_{\mathbf{z} \in Z_t} \frac{p_d(\mathbf{x}) g(\mathbf{z}_t|\mathbf{x}) \bar{v}_t(\mathbf{x})}{c(\mathbf{z}) + \int p_d(\zeta) g(\mathbf{z}_t|\zeta) \bar{v}_t(\zeta) d\zeta}, \quad (11)$$

where $p_d(\mathbf{x})$, $g(\mathbf{z}_t|\mathbf{x})$, and $c(\mathbf{z})$ are the probability of detection, likelihood function, and clutter model of the sensor

respectively [30]. By using this recursion, the swarm probabilistic description can be updated. The recursion itself avoids computations that arise from the unknown relation between agents and its measurements, and that the posterior intensity is a function of a single-agent's state space. Unfortunately, Eqs. (10) and (11) do not contain a closed-form solution and the numerical integration suffers from higher computational time as the state increases due to an increasing number of agents.

D. Gaussian Mixture Model and Control Formulation

Fortunately, a closed-form solution exists if it is assumed that the survival and detection probabilities are state independent (i.e. $p_s(\mathbf{x}) = p_s$ and $p_d(\mathbf{x}) = p_d$), and the intensities of the birth and spawn RFSs are Gaussian mixtures. To formulate the optimal control problem, the current intensity and desired intensity are

$$\bar{\nu}(\mathbf{x}, k) \triangleq \sum_{i=1}^{N_f} w_f^{(i)} \mathcal{N}(\mathbf{x}; \mathbf{m}_f^i, P_f^i) \triangleq \nu_b(\mathbf{x}, k) + \nu_{p_s}(\mathbf{x}, k) + \nu_\beta(\mathbf{x}, k), \quad (12)$$

$$\nu_{des}(\mathbf{x}, k) = g(\mathbf{x}) \triangleq \sum_{i=1}^{N_g} w_g^{(i)} \mathcal{N}(\mathbf{x}; \mathbf{m}_g^i, P_g^i), \quad (13)$$

where $w^{(i)}$ are the weights and $\mathcal{N}(\mathbf{x}; \mathbf{m}^i, P^i)$ is the probability density function of a i th multivariate Gaussian distribution with a mean and covariance corresponding to the peaks and spread of the intensity respectively. It is assumed that the desired Gaussian mixture intensity, $\nu_{des}(\mathbf{x}, k)$, is known. Eq. (12) includes the summation of the individual birth ($\nu_b(\mathbf{x}, k)$), spawn (ν_β), and survival ($\nu_{p_s}(\mathbf{x}, k)$) Gaussian mixture intensities which simplify to another Gaussian mixture. Note that closed form solutions using Gaussian mixtures exist for cases without the state independent assumption. Additionally, $\sum_{i=1}^{N_f} w_f^{(i)} = N_{total}(t)$ and $\sum_{i=1}^{N_g} w_g^{(i)} = \bar{N}_{total}(t)$ where $\bar{N}_{total}(t)$ is the desired number of agents. The intensity function $\nu(\mathbf{x}, t)$ is in terms of the swarm state while $\nu_{des}(\mathbf{x}, t)$ is in terms of the desired state. The swarm intensity function can be propagated through updates on the mean and covariance of the Gaussian mixtures as given by

$$\mathbf{m}_{f,k+1}^i = A_k \mathbf{m}_{f,k}^i + B_k \mathbf{u}_{f,k}^i, \quad (14)$$

$$P_{f,k+1}^i = A_k P_{f,k}^i A_k^T + Q_k, \quad (15)$$

where Q_k is process noise. The agents' states \mathbf{x} are incorporated in the mean and covariance of the Gaussian mixture intensity. Then given the Gaussian mixture intensities assumption, a control variable is calculated for each component $\mathbf{u}_{f,k}^i$. Additionally, each Gaussian mixture component represents many agents since the intensity function integrates to the total number of agents. Note that although linear dynamics is used, the dynamics can be considered where the policy is a nonlinear function of the state.

Additionally, the measurement update is also closed form given by the intensity

$$v_k(\mathbf{x}, k) = f(\mathbf{x}) = (1 - p_d(\mathbf{x}))\bar{v}_k(\mathbf{x}) + \sum_{\mathbf{z} \in Z_k} \sum_{j=1}^{N_f} w_k^{(j)} \mathcal{N}(\mathbf{x}; \mathbf{m}_{k|k}^{(j)}(\mathbf{z}), P_{k|k}^{(j)}), \quad (16)$$

where

$$w_k^{(j)} = \frac{p_d(\mathbf{x})w_f^{(j)}q^{(j)}(\mathbf{z})}{K(\mathbf{z}) + p_d(\mathbf{x})\sum_{l=1}^{N_f} w_f^{(l)}q^{(l)}(\mathbf{z})}, \quad (17a)$$

$$\mathbf{m}_{k|k}^{(j)}(\mathbf{z}) = \mathbf{m}_f^{(j)} + K^{(j)}(\mathbf{z} - H_k \mathbf{m}_f^{(j)}), \quad (17b)$$

$$P_{k|k}^{(j)} = (I - K^{(j)}H_k)P_f^i, \quad (17c)$$

$$K^{(j)} = P_f^i H_k^T (H_k P_f^i H_k^T + R_k)^{-1}, \quad (17d)$$

$$q_k^{(j)}(\mathbf{z}) = \mathcal{N}(\mathbf{z}; H_k \mathbf{m}_f^{(j)}, R_k + H_k P_f^i H_k^T), \quad (17e)$$

which follow closely to the Kalman filter measurement update equations.

Each individual swarm agent runs a local PHD observer to estimate the state of the swarm by modeling the swarm as a distribution. Thus, using RFS theory, it is assumed that the individual swarm agents form an intensity function that is a Gaussian mixture intensity in which the means and covariances of the Gaussian mixture are propagated and controlled. An optimal control problem is set up that tracks a desired swarm formation by minimizing its control effort in the following objective function

$$J(\mathbf{u}) = \int_0^T E \{ \mathbf{u}(t)^T R \mathbf{u}(t) \} + D(v(\mathbf{x}, t), v_{des}(\mathbf{x}, t)) dt, \quad (18)$$

where $v_{des}(\mathbf{x}, t)$ is the desired formation, R is the positive definite control weight matrix, and $\mathbf{u}(t)$ is the control effort for the Gaussian mixture intensities shown in Eq. (14). Both $v(\mathbf{x}, t)$ and $v_{des}(\mathbf{x}, t)$ are defined over the complete state space which include position and velocity parameters. $D(v(\mathbf{x}, t), \bar{v}(\mathbf{x}, t))$ is the distance between these Gaussian mixtures which has several closed-form solutions, and it was used previously to define an objective function for path planning of multi-agent systems [9].

The key features that RFS for the control problem of swarming agents is that it can allow for a unified representation for swarming systems. This unified representation is achieved by minimizing the RFS objective function, Eq. (18), about the swarm intensity statistics given by Eq. (14) and (15). Thus, it can handle multi-fidelity swarm localization and control. The swarm is treated probabilistically and the bulk motion is modeled which allows the theory to handle large numbers of indistinguishable units with unknown swarm size. This reduces the dimensionality of the state while enabling complex behavior. Naturally, the RFS control problem is formulated to enable complex distributed decision

making through RFS theory.

III. Distributional Distance Based-Cost

The control objective for the RFS formulation of agents with an unknown distance between the intensities is provided by Eq. (18). The distance metric can be defined using several closed-form solutions for Gaussian mixtures. Then, the corresponding optimal control problem is formulated using several closed-form methods discussed in the next section.

A. Cauchy-Schwarz Divergence

The Cauchy-Schwarz divergence is based on the Cauchy-Schwarz inequality for inner products of RFS, and it is defined for two RFS with intensities f and g given by

$$D_{CS}(f, g) = -\ln\left(\frac{\langle f, g \rangle}{\|f\| \|g\|}\right), \quad (19)$$

where $\langle \cdot, \cdot \rangle$ is the L_2^2 inner product over the RFS intensities. The argument of the logarithm is non-negative since probability densities are non-negative, and it does not exceed one by the Cauchy-Schwarz inequality. The Cauchy-Schwarz divergence can be interpreted as an approximation to the Kullback-Leibler divergence but has a closed-form expression for Gaussian mixtures [32]. This is useful for calculating the distance between two-point processes represented by intensity functions. By substituting the intensities from Eq. (16) and Eq. (13) for f and g respectively, the Cauchy-Schwarz divergence between two Poisson point processes with Gaussian mixture intensities, $D_{CS}(f, g)$, is simplified to

$$\begin{aligned} D_{CS}(f, g) = & \frac{1}{2} \ln\left(\sum_{j=1}^{N_f} \sum_{i=1}^{N_f} w_f^{(j)} w_f^{(i)} \mathcal{N}(\mathbf{m}_f^j; \mathbf{m}_f^i, P_f^i + P_f^j)\right) \\ & + \frac{1}{2} \ln\left(\sum_{j=1}^{N_g} \sum_{i=1}^{N_g} w_g^{(j)} w_g^{(i)} \mathcal{N}(\mathbf{m}_g^j; \mathbf{m}_g^i, P_g^i + P_g^j)\right) \\ & - \ln\left(\sum_{j=1}^{N_g} \sum_{i=1}^{N_f} w_g^{(j)} w_f^{(i)} \mathcal{N}(\mathbf{m}_g^j; \mathbf{m}_f^i, P_g^i + P_f^j)\right). \end{aligned} \quad (20)$$

Note that in the control formulation used, only $v(\mathbf{x}, t)$ is assumed to depend on the control \mathbf{u} . Therefore, the term that depends only on $\bar{v}(\mathbf{x}, t)$ is omitted from the objective function since $\bar{v}(\mathbf{x}, t)$ does not depend on \mathbf{u} .

Figure 1(a) shows the surface plot using the Cauchy-Schwarz divergence for four intensities in the swarm at an initial time instance. The four intensities start with initial conditions of $(\pm 3, \pm 3)$ in a square grid. The target destinations were set as $(\pm 1, \pm 1)$ in a square grid. From the surface plot, each initial state has hills while the destination states have valleys. Therefore in the minimization of the objective function, each intensity will repel each other while moving towards the final state through time. If the initial state is too large compared to the destination states, it will take longer for the four intensities to converge to the destination values or diverge due to the optimization getting stuck in local minima (the flat

plane). Also, the repelling effect due to the hills are relatively small. Thus, the Cauchy-Schwarz divergence may not be the fastest converging solution for the objective function minimization.

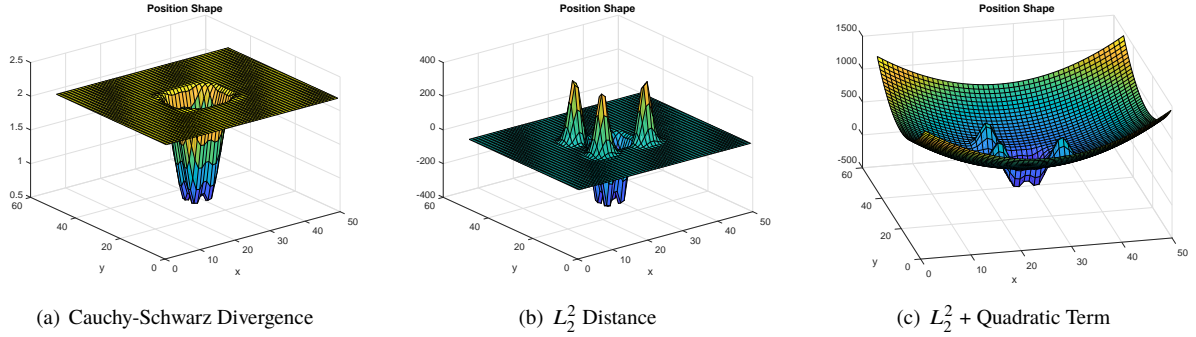


Fig. 1 Surface Plots of the RFS divergences.

B. L_2^2 Distance

Alternatively, the distance between two Poisson point processes with Gaussian mixture intensities can be determined by using the L_2^2 distance between the intensities. The L_2^2 is given by

$$D_{L_2^2}(f, g) = \int (f - g)^2 d\mathbf{x} = \|f - g\|^2, \quad (21)$$

where the close-form solution for Gaussian mixture intensities is simplified to

$$\begin{aligned} D_{L_2^2}(f, g) &= \sum_{j=1}^{N_f} \sum_{i=1}^{N_f} w_f^{(j)} w_f^{(i)} \mathcal{N}(\mathbf{m}_f^j; \mathbf{m}_f^i, P_f^i + P_f^j) \\ &+ \sum_{j=1}^{N_g} \sum_{i=1}^{N_g} w_g^{(j)} w_g^{(i)} \mathcal{N}(\mathbf{m}_g^j; \mathbf{m}_g^i, P_g^i + P_g^j) \\ &- 2 \sum_{j=1}^{N_g} \sum_{i=1}^{N_f} w_g^{(j)} w_f^{(i)} \mathcal{N}(\mathbf{m}_g^j; \mathbf{m}_f^i, P_g^i + P_f^j). \end{aligned} \quad (22)$$

The L_2^2 distance is stationary, i.e. gradients are zero, when intensities f and g are equal. That is, the cost is minimum when the target g is reached from any intensity f .

The L_2^2 distance follows the property of the Bregman divergence which has an additional property of convexity [33]. The distance, given by

$$D_F(f, g) = F(f) - F(g) - \langle \nabla F(g), f - g \rangle, \quad (23)$$

is convex if $F(\cdot)$ is strictly convex and continuously differentiable on a closed convex set [33]. A list of strictly convex functions are listed in [33]. For this work, the squared Euclidean distance $F(f) = f^2$ was used to generate the Bregman

divergence given by

$$D_F(f, g) = \langle f, f \rangle + \langle g, g \rangle - 2 \langle f, g \rangle, \quad (24)$$

which is in the same exact form of Eq. (22). Figure 1(b) shows the surface plot using the L_2^2 distance for a 4-intensity swarm for the same example as the Cauchy-Schwarz divergence. Each initial state has more defined hills compared to the Cauchy-Schwarz divergence. Thus, the initial states have a stronger repel effect from each other. Also, the destination states have large valleys that create a large attraction effect for each initial state to move to. Thus, the optimization solution will be faster in the L_2^2 distance case. Unfortunately, the L_2^2 distance suffers from a similar issue to the Cauchy-Schwarz divergence. If the initial conditions increase farther away from the destination states, the optimization may take much longer or get stuck in local minima due to a flat surface away from the destination states.

C. L_2^2 Distance with Quadratic Term

The issue of convergence remains for the L_2^2 distance when the initial states are farther away from the destination states. To achieve faster convergence, an additional term is added to the L_2^2 distance to shape the gradient descent through a quadratic term as given by

$$D_{L_2^2 mod}(f, g) = D_{L_2^2}(f, g) - \alpha \sum_{j=1}^{N_g} \sum_{i=1}^{N_f} w_g^{(j)} w_f^{(i)} \ln \left(\mathcal{N}(\mathbf{m}_g^j; \mathbf{m}_f^i, P_g^i + P_f^j) \right), \quad (25)$$

where α is a fixed or changing parameter. Unfortunately, adding the quadratic term to the L_2^2 distance does not make the objective function stationary at $f = g$. To alleviate this issue, the α parameter is included with the quadratic term to relax the contribution of the gradient to the L_2^2 stationary point. By substituting Eq. (22) into Eq. (25), the equation becomes

$$\begin{aligned} D_{L_2^2 mod}(f, g) &= \sum_{j=1}^{N_f} \sum_{i=1}^{N_f} w_f^{(j)} w_f^{(i)} \mathcal{N}(\mathbf{m}_f^j; \mathbf{m}_f^i, P_f^i + P_f^j) \\ &+ \sum_{j=1}^{N_g} \sum_{i=1}^{N_g} w_g^{(j)} w_g^{(i)} \mathcal{N}(\mathbf{m}_g^j; \mathbf{m}_g^i, P_g^i + P_g^j) \\ &- 2 \sum_{j=1}^{N_g} \sum_{i=1}^{N_f} w_g^{(j)} w_f^{(i)} \mathcal{N}(\mathbf{m}_g^j; \mathbf{m}_f^i, P_g^i + P_f^j) \\ &- \alpha \sum_{j=1}^{N_g} \sum_{i=1}^{N_f} w_g^{(j)} w_f^{(i)} \ln \left(\mathcal{N}(\mathbf{m}_g^j; \mathbf{m}_f^i, P_g^i + P_f^j) \right). \end{aligned} \quad (26)$$

Note that this term is referred as quadratic, although it may be more appropriate to call it quadratic-like. Figure 1(c) shows the surface plot using Eq. (26) for the same 4-intensity swarm used in the Cauchy-Schwarz divergence. Compared to the L_2^2 distance, the initial and destination states provide the hills and valleys necessary to obtain convergence. However, as the initial states move outwards, the surface map decreases in a quadratic fashion instead of staying flat. This

prevents the optimization from converging to a local minima. Instead, the additional quadratic term allows convergence to the destination states (global minima). Thus, the optimization can occur at any point to reach convergence in a timely manner.

Traditional LQR based solutions are not applicable to the minimization of the objective function, Eq. (26), since the L_2^2 terms are nonquadratic [31]. The minimization of the objective function in discrete time is

$$\begin{aligned}
\min_{\mathbf{u}_k, k=1, \dots, T} J(\mathbf{u}) &= \sum_{k=1}^T E\{\mathbf{u}_k^T R \mathbf{u}_k\} + \sum_{j=1}^{N_f} \sum_{i=1}^{N_f} w_{f,k}^{(j)} w_{f,k}^{(i)} \mathcal{N}(\mathbf{m}_{f,k}^j; \mathbf{m}_{f,k}^i, P_{f,k}^i + P_{f,k}^j) \\
&+ \sum_{j=1}^{N_g} \sum_{i=1}^{N_g} w_{g,k}^{(j)} w_{g,k}^{(i)} \mathcal{N}(\mathbf{m}_{g,k}^j; \mathbf{m}_{g,k}^i, P_{g,k}^i + P_{g,k}^j) \\
&- 2 \sum_{j=1}^{N_g} \sum_{i=1}^{N_f} w_{g,k}^{(j)} w_{f,k}^{(i)} \mathcal{N}(\mathbf{m}_{g,k}^j; \mathbf{m}_{f,k}^i, P_{g,k}^i + P_{f,k}^j) \\
&- \alpha \sum_{j=1}^{N_g} \sum_{i=1}^{N_f} w_{g,k}^{(j)} w_{f,k}^{(i)} \ln \left(\mathcal{N}(\mathbf{m}_{g,k}^j; \mathbf{m}_{f,k}^i, P_{g,k}^i + P_{f,k}^j) \right),
\end{aligned} \tag{27}$$

$$\text{Subject to : } \mathbf{m}_{f,k+1}^i = A_k \mathbf{m}_{f,k}^i + B_k \mathbf{u}_{f,k}^i, \tag{28}$$

where $\mathbf{u}_k = [(\mathbf{u}_{f,k}^1)^T, \dots, (\mathbf{u}_{f,k}^{N_f})^T]^T$ is the collection of all control variables. Therefore, control solutions are found by either using ILQR where the objective function is quadratized by taking a Taylor series approximation about a nominal trajectory or using model predictive control where solutions to the nonquadratic objective function are found using optimization techniques.

IV. Iterative LQR

The LQR finite-horizon optimal control is first discussed in Section IV.A in order to provide the necessary background to approach ILQR control for general nonlinear system dynamics and a nonquadratic objective function discussed in Section IV.B.

A. LQR Finite-Horizon Optimal Control Problem

The linear quadratic regulator problem is defined by a discrete time-varying system given by

$$\mathbf{x}_{k+1} = A_k \mathbf{x}_k + B_k \mathbf{u}_k + \mathbf{g}_k, \tag{29}$$

where \mathbf{g}_k is Brownian process noise. For the finite horizon N , the total cost is calculated from initial state \mathbf{x}_0 and the control sequence $U = [\mathbf{u}_k, \mathbf{u}_{k+1}, \dots, \mathbf{u}_{N-1}]$ applied to the dynamics given by

$$J(\mathbf{x}_0, U) = \sum_{k=0}^{N-1} l(\mathbf{x}_k, \mathbf{u}_k) + l_f(\mathbf{x}_N), \quad (30)$$

where $l(\mathbf{x}_k, \mathbf{u}_k)$ is the running cost and $l_f(\mathbf{x}_N)$ is the terminal cost. The LQR costs are quadratic given by

$$l(\mathbf{x}_k, \mathbf{u}_k) = \frac{1}{2} \begin{bmatrix} 1 \\ \mathbf{x}_k \\ \mathbf{u}_k \end{bmatrix}^T \begin{bmatrix} 0 & \mathbf{q}_k^T & \mathbf{r}_k^T \\ \mathbf{q}_k & Q_k & P_k \\ \mathbf{r}_k & P_k & R_k \end{bmatrix} \begin{bmatrix} 1 \\ \mathbf{x}_k \\ \mathbf{u}_k \end{bmatrix}, \quad l_f(\mathbf{x}_N) = \frac{1}{2} \mathbf{x}_N^T Q_N \mathbf{x}_N + \mathbf{x}_N^T \mathbf{q}_N + c, \quad (31)$$

where \mathbf{q}_k , \mathbf{r}_k , Q_k , R_k , and P_k are the running weights (coefficients), Q_N and \mathbf{q}_N are the terminal weights, and c is a constant for the quadratic expansion. The weight matrices, Q_k and R_k , are positive definite and the block matrix $\begin{bmatrix} Q_k & P_k \\ P_k & R_k \end{bmatrix}$ is positive-semidefinite [34]. The running and terminal costs are substituted into Eq. (30), and due to the symmetry in the weight matrices, the total cost is simplified to

$$J(\mathbf{x}_0, U) = \sum_{k=0}^{N-1} \mathbf{x}_k^T \mathbf{q}_k + \mathbf{u}_k^T \mathbf{r}_k + \frac{1}{2} \mathbf{x}_k^T Q_k \mathbf{x}_k + \frac{1}{2} \mathbf{u}_k^T R_k \mathbf{u}_k + \mathbf{u}_k^T P_k \mathbf{x}_k + \frac{1}{2} \mathbf{x}_N^T Q_N \mathbf{x}_N + \mathbf{x}_N^T \mathbf{q}_N + c. \quad (32)$$

The optimal control solution is based on minimizing the cost function in terms of the control sequence which is given by

$$U^*(\mathbf{x}_0) = \min_U J(\mathbf{x}_0, U). \quad (33)$$

To solve for the optimal control solution given by Eq. (33), a value iteration method is used. Value iteration is a method that determines the optimal cost-to-go (value) starting at the final time-step and moving backwards in time minimizing the control sequence. The cost-to-go is defined as

$$J(\mathbf{x}_k, U_k) = \sum_k^{N-1} l(\mathbf{x}_k, \mathbf{u}_k) + l_f(\mathbf{x}_N), \quad (34)$$

where $U_k = [\mathbf{u}_k, \mathbf{u}_{k+1}, \dots, \mathbf{u}_{N-1}]$. This is very similar to Eq. (30), but the only difference is that the cost starts from time-step k instead of $k = 0$. The optimal cost-to-go is calculated similar to Eq.(33) which is

$$V(\mathbf{x}_k) = \min_{U_k} J(\mathbf{x}_k, U_k). \quad (35)$$

At a time-step k , the optimal cost-to-go function is a quadratic function given by

$$V(\mathbf{x}_k) = \frac{1}{2} \mathbf{x}_k^T S_k \mathbf{x}_k + \mathbf{x}_k^T \mathbf{s}_k + c_k, \quad (36)$$

where S_k , \mathbf{s}_k , and c_k are computed backwards in time using the value iteration method. First, the final conditions $S_N = Q_N$, $\mathbf{s}_N = \mathbf{q}_N$, and $c_N = c$ are set. This reduces the minimization of the entire control sequence to just a minimization over a control input at a time-step which is the principle of optimality [35]. To find the optimal cost-to-go, the Riccati equations are used to propagate the final conditions backwards in time given by

$$S_k = A_k^T S_{k+1} A_k + Q_k - \left(B_k^T S_{k+1} A_k + P_k^T \right)^T \left(B_k^T S_{k+1} B_k + R_k \right)^{-1} \left(B_k^T S_{k+1} A_k + P_k^T \right), \quad (37a)$$

$$\begin{aligned} \mathbf{s}_k &= \mathbf{q}_k + A_k^T \mathbf{s}_{k+1} + A_k^T S_{k+1} \mathbf{g}_k \\ &\quad - \left(B_k^T S_{k+1} A_k + P_k^T \right)^T \left(B_k^T S_{k+1} B_k + R_k \right)^{-1} \left(B_k^T S_{k+1} \mathbf{g}_k + B_k^T \mathbf{s}_{k+1} + \mathbf{r}_k \right), \end{aligned} \quad (37b)$$

$$\begin{aligned} c_k &= \mathbf{g}_k^T S_{k+1} \mathbf{g}_k + 2 \mathbf{s}_{k+1}^T \mathbf{g}_k + c_{k+1} \\ &\quad - \left(B_k^T S_{k+1} \mathbf{g}_k + B_k^T \mathbf{s}_{k+1} + \mathbf{r}_k \right)^T \left(B_k^T S_{k+1} B_k + R_k \right)^{-1} \left(B_k^T S_{k+1} \mathbf{g}_k + B_k^T \mathbf{s}_{k+1} + \mathbf{r}_k \right). \end{aligned} \quad (37c)$$

Using the Riccati solution, the optimal control policy is in the affine form

$$\mathbf{u}_k(\mathbf{x}_k) = K_k \mathbf{x}_k + \mathbf{l}_k, \quad (38)$$

where K_k is the controller given by

$$K_k = -(R_k + B_k^T S_{k+1} B_k)^{-1} (B_k^T S_{k+1} A_k + P_k^T), \quad (39)$$

and \mathbf{l}_k is the controller offset given by

$$\mathbf{l}_k = -(R_k + B_k^T S_{k+1} B_k)^{-1} (B_k^T S_{k+1} \mathbf{g}_k + B_k^T \mathbf{s}_{k+1} + \mathbf{r}_k). \quad (40)$$

This optimal solution to the LQR problem works for linear dynamics and quadratic cost functions, but unfortunately, the objective function specified for the swarm problem is nonquadratic. Fortunately, an iterative LQR can be used for nonlinear dynamics and nonquadratic local cost functions.

B. Iterative LQR Problem

The ILQR approach to solving nonlinear and nonquadratic equations uses the same process as the LQR solution, but the dynamics and objective function are linearized and quadratized and the LQR solution is iterated to increasingly get better approximations of the optimal trajectory of the system. The following discussion on ILQR follows closely to that of Tassa [36]. The general nonlinear discrete-time dynamics is given by

$$\mathbf{x}_{k+1} = f(\mathbf{x}_k, \mathbf{u}_k), \quad (41)$$

where the state at the next time-step, \mathbf{x}_{k+1} , is a function of the current state, \mathbf{x}_k , and control input \mathbf{u}_k . The cost function is in the form of Eq. (30), but the costs are nonquadratic. The solution to the optimal control problem is Eq. (33). Similarly, the cost-to-go and the optimal cost-to-go function are defined by Eq. (34) and Eq. (35) respectively. By setting the terminal condition $V(\mathbf{x}_N) = l_f(\mathbf{x}_N)$, the principle of optimality is used to minimize over the control at a time-step given by

$$V(\mathbf{x}_k) = \min_{\mathbf{u}_k} (l(\mathbf{x}_k, \mathbf{u}_k) + V(\mathbf{x}_{k+1})), \quad (42)$$

and solved through time by a backwards pass (value iteration).

1. Backward Pass

The first step in the backward pass (value iteration) is to determine a value function that is quadratic. The argument in Eq. (42) is taken as a function of small perturbations around the state ($\delta\mathbf{x}_k$) and control input ($\delta\mathbf{u}_k$), and it is quadratized through a second order Taylor series expansion given by

$$\begin{aligned} Q(\delta\mathbf{x}, \delta\mathbf{u}) &= l(\mathbf{x}_k + \delta\mathbf{x}_k, \mathbf{u}_k + \delta\mathbf{u}_k) - l(\mathbf{x}, \mathbf{u}) + V(\mathbf{x}_{k+1} + \delta\mathbf{x}_{k+1}) - V(\mathbf{x}_{k+1}), \\ &\approx \frac{1}{2} \begin{bmatrix} 1 \\ \delta\mathbf{x}_k \\ \delta\mathbf{u}_k \end{bmatrix}^T \begin{bmatrix} 0 & Q_x^T & Q_u^T \\ Q_x & Q_{xx} & Q_{xu} \\ Q_u & Q_{ux} & Q_{uu} \end{bmatrix} \begin{bmatrix} 1 \\ \delta\mathbf{x}_k \\ \delta\mathbf{u}_k \end{bmatrix}, \end{aligned} \quad (43)$$

where Q_x , Q_u , Q_{xx} , Q_{xu} , and Q_{uu} are the running coefficients (weights) of the quadratized value function at a certain time-step. Note, in the standard formulation, the time-step k is dropped for these equations. Any primes denote the next time-step. The equations for the running weights are given by

$$Q_x = l_x + f_x^T V'_x, \quad (44a)$$

$$Q_u = l_u + f_u^T V'_x, \quad (44b)$$

$$Q_{xx} = l_{xx} + f_x^T V'_{xx} f_x + V'_x f_{xx}, \quad (44c)$$

$$Q_{uu} = l_{uu} + f_u^T V'_{xx} f_u + V'_x f_{uu}, \quad (44d)$$

$$Q_{ux} = l_{ux} + f_u^T V'_{xx} f_x + V'_x f_{ux}, \quad (44e)$$

where l_x, l_u, l_{xx}, l_{uu} , and l_{ux} are the gradients and Hessians of the cost function, $f_x, f_u, f_{xx}, f_{uu}, f_{ux}$ are the gradients and Hessians of the nonlinear dynamics, and V'_x , and V'_{xx} are the gradient and Hessian of the value function. For the ILQR formulation, the Hessians of the nonlinear dynamics are ignored. By using this quadratic approximation, the minimum in terms of $\delta \mathbf{u}$ is found given by

$$\delta \mathbf{u} = \min_{\delta \mathbf{u}} Q(\delta \mathbf{x}, \delta \mathbf{u}) = -Q_{uu}^{-1} (Q_u + Q_{ux} \delta \mathbf{x}), \quad (45)$$

which give local feedback and feed-forward gains of

$$K = -Q_{uu}^{-1} Q_{ux}, \quad (46a)$$

$$\mathbf{k} = -Q_{uu}^{-1} Q_u, \quad (46b)$$

respectively. The locally optimal controller is substituted back into Eq. (43) to get the optimal value at a time-step k given by

$$\Delta V = -\frac{1}{2} \mathbf{k}^T Q_{uu} \mathbf{k}, \quad (47a)$$

$$V_x = Q_x - K^T Q_{uu} \mathbf{k}, \quad (47b)$$

$$V_{xx} = Q_{xx} - K^T Q_{uu} K, \quad (47c)$$

so the value can be propagated backwards in time to find new locally optimal solutions to the value function.

2. Forward Pass

By continually computing the quadratic approximations in Eq. (44), local controller in Eq. (46), and the new values in Eq. (47) backwards in time from the terminal condition $V(\mathbf{x}_N) = l_f(\mathbf{x}_N)$, the newly controlled trajectory can be found through a forward pass given by

$$\hat{\mathbf{x}}_0 = \mathbf{x}_0, \quad (48a)$$

$$\hat{\mathbf{u}}_k = \mathbf{u}_k + \mathbf{k}_k + K_k (\hat{\mathbf{x}}_k - \mathbf{x}_k), \quad (48b)$$

$$\hat{\mathbf{x}}_{k+1} = f(\hat{\mathbf{x}}_k, \hat{\mathbf{u}}_k). \quad (48c)$$

where $\hat{\mathbf{x}}_k$ and $\hat{\mathbf{u}}_k$ consists the state and control input at a time-step of the new trajectory $(\hat{\mathbf{X}}, \hat{\mathbf{U}})$. This composes one iteration of ILQR. If the cost of the new trajectory, $(\hat{\mathbf{X}}, \hat{\mathbf{U}})$, is less than the cost of the old trajectory, (\mathbf{X}, \mathbf{U}) , then $\mathbf{X} = \hat{\mathbf{X}}$ and $\mathbf{U} = \hat{\mathbf{U}}$ are set, and the algorithm is ran again until a convergence threshold is met between the old and new costs.

3. Regularization via the Levenberg-Marquardt Heuristic

If the cost of the new trajectory is greater than the cost of the old trajectory, the iteration has not provided a better solution. To circumvent this issue, regularization onto the Hessian is implemented into the problem. This is called the Levenberg-Marquardt heuristic. The control sequence that is calculated in ILQR is computed like a Newton optimization which uses second order information (curvature information) on top of the first order information (gradient information) [37]. By including second order curvature to the update, optimization can occur faster, but this relies on the fact that the Hessian is positive definite and an accurate quadratic model. If the control update is not improving (for a non-positive definite Hessian and inaccurate quadratic model), the Levenberg-Marquardt heuristic uses less curvature information and more on the gradient information. This regularization is added to the Hessian of the control cost given by

$$\tilde{Q}_{uu} = Q_{uu} + \mu I_m, \quad (49)$$

where \tilde{Q}_{uu} is the regularized control cost Hessian, μ is the Levenberg-Marquardt parameter, and I_m is the identity matrix that is the size of the control input vector [38]. This allows the increase or decrease of using curvature information in the optimization by adding a quadratic cost around the current control input. Unfortunately, adding this regularization term can have different effects at different time-steps using the same control perturbation based on a changing f_u in the linearized dynamics. By increasing $\mu \rightarrow \infty$, the \mathbf{k} and K gains become very small due to the \tilde{Q}_{uu}^{-1} term. Therefore, the regularization term is improved by penalizing the states instead of the control inputs which is given by

$$\tilde{Q}_{uu} = l_{uu} + f_u^T (V'_{xx} + \mu I_n) f_u + V'_x f_{uu}, \quad (50a)$$

$$\tilde{Q}_{ux} = l_{ux} + f_u^T (V'_{xx} + \mu I_n) f_x + V'_x f_{ux}, \quad (50b)$$

$$K = -\tilde{Q}_{uu}^{-1} \tilde{Q}_{ux}, \quad (50c)$$

$$\mathbf{k} = -\tilde{Q}_{uu}^{-1} Q_u, \quad (50d)$$

where I_n is the identity matrix that is the size of the state vector. The μ parameter is placed on the state instead of the control input. For this method, the regularization term is directly incorporated with f_u , and the feedback gains, \mathbf{k} and K , do not disappear as $\mu \rightarrow \infty$. Instead, the new \mathbf{k} and K values bring the new trajectory closer to the old one. For the implementation of the μ term, three requirements should be followed. If reaching the minimum is accurate, the μ should

become zero in order to obtain faster convergence due to the second order optimization term. If a non-positive definite \tilde{Q}_{uu} is found, the backward pass should be restarted with a larger μ . The last requirement is when a $\mu > 0$ is needed, the smallest μ should be used that allows the \tilde{Q}_{uu} to be positive definite. Therefore, more of the second order information can be used to provide faster convergence than using gradient descent.

Eq. (47) must also be modified based on regularization added in Eq. (50a) [31]. Eq. (47) was originally derived using Eqs. (43) and (45), but using the new regularized terms in Eq. (50a) creates error. Therefore, the modified values at a time-step k is

$$\Delta V = \frac{1}{2} \mathbf{k}^T Q_{uu} \mathbf{k} + \mathbf{k}^T Q_u, \quad (51a)$$

$$V_x = Q_x + K^T Q_{uu} \mathbf{k} + K^T Q_u + Q_{ux}^T \mathbf{k}, \quad (51b)$$

$$V_{xx} = Q_{xx} + K^T Q_{uu} K + K^T Q_{ux} + Q_{ux}^T K. \quad (51c)$$

The regularization terms create a faster and more accurate solution to the backwards pass of the ILQR solution.

4. Forward Pass Line Search

Regularization of the forward pass can improve convergence and performance of the ILQR algorithm. For linear time-varying systems, one iteration provides a minimal solution after one iteration. This is not the case for general nonlinear systems. Since, nonlinear systems are linearized by a Taylor series approximation, there may be regions in the new ILQR trajectory that are not valid about the nonlinear model. This may lead to divergence and have a larger cost function than the old trajectory. To fix this issue, a backtracking line-search parameter is introduced in the control update equation given by

$$\hat{\mathbf{u}}_k = \mathbf{u}_k + \alpha \mathbf{k}_k + K_k (\hat{\mathbf{x}}_k - \mathbf{x}_k), \quad (52)$$

where α is set to $\alpha = 1$ at the start of the forward pass. Then the expected cost reduction is considered using

$$\Delta J(\alpha) = \alpha \sum_{k=0}^{N-1} \mathbf{k}(k)^T Q_u(k) + \frac{\alpha^2}{2} \sum_{k=0}^{N-1} \mathbf{k}^T(k) Q_{uu}(k) \mathbf{k}(k). \quad (53)$$

A ratio z is determined using the actual and expected cost reduction given by

$$z = \frac{\left(J(\mathbf{x}_0, U) - J(\hat{\mathbf{x}}_0, \hat{U}) \right)}{\Delta J(\alpha)}, \quad (54)$$

where $J(\mathbf{x}_0, U)$ and $J(\hat{\mathbf{x}}_0, \hat{U})$ are the old and new cost respectively. The control update is accepted if the condition given by

$$0 < c_1 < z, \quad (55)$$

is met where c_1 is a parameter set by the user. The c_1 is usually set close to zero. If the condition is not met, the forward pass is restarted with a smaller α value which means that the new trajectory strayed farther than the system's region of validity. By using the α line search parameter, convergence can be achieved for nonlinear systems by iteratively decreasing α to obtain a cost reduction.

5. ILQR Summary

An ILQR iteration can be summarized in four steps. First, an initial rollout of the nonlinear dynamics given by Eq. (41) is integrated over time for a given control sequence U . If there is no good initialization of the control sequence, the control sequence can be set to $U = 0$. After the initial rollout, the derivatives of the cost function and nonlinear dynamics used in Eq. (44) are found. The derivatives are used in the third step which is to determine local control solutions using a backward pass. Using the terminal condition, $V(\mathbf{x}_N) = l_f(\mathbf{x}_N)$, local control solutions are found by iterating Eq. (44), (50), and (51) backwards at each time-step. When a non-positive definite \tilde{Q}_{uu} is found, increase the regularization parameter μ and restart the backward pass. Once, a local optimal policy is found, α is set to $\alpha = 1$, and Eqs. (53) and (48c) are propagated forward in time. If the integration diverged or cost reduction condition in Eq. (55) was not met, the forward pass is restarted with a smaller α .

V. Receding Horizon Dynamic Programming

An optimal solution can also be obtained by minimizing the objective, Eq. (26), using MPC or receding horizon control [26]. The MPC approach uses dynamic programming techniques to obtain an optimal control solution \mathbf{u} from the objective function.

Conceptually, at a time k , the knowledge of the system model is used to derive a sequence $\mathbf{u}(k|k), \mathbf{u}(k+1|k), \mathbf{u}(k+2|k), \dots, \mathbf{u}(k+T_p|k)$ where T_p is the finite prediction horizon from the current state $\bar{\mathbf{x}}(k)$ [39]. With the input sequence, the state is moved forward in time by the control horizon, T_c ; usually one time-step. Then the same strategy is repeated for time $k+1$. T_p can be chosen to be either small or large. As T_p increases, the degrees of freedom in the optimization increases which can slow down the algorithm considerably even though more of the future reference trajectory would be useful to bring the output closer to the reference. With a smaller T_p , the computation time will be faster, but the optimization may be more suboptimal. Thus, the swarm may not converge to the desired configuration.

VI. Control using RFS Formulation

For the RFS control formulation, a \mathbf{u} that controls the swarm intensities through their statistics (mean and covariance) is found by minimizing the objective as given by Eq. (27) and (28). This was done using ILQR and MPC. ILQR is able to determine an optimal solution, to an objective function, for nonlinear equations of motion and nonquadratic cost function through an iterative process of finding the LQR solution involving linearization and quadratization. For MPC,

the optimal control input \mathbf{u} is found using MATLAB's `fminunc` solver and the Quasi-Newton algorithm [40]. Note that ILQR and MPC are both closed-loop control methods in terms of the statistics (mean and covariance) of the system. Then, the agents in the swarm were initialized to the closest intensity using the Mahalanobis distance given by

$$D_M(\mathbf{x}, \mathbf{m}_{f,k}^i) = \sqrt{(\mathbf{x} - \mathbf{m}_{f,k}^i)^T P^{-1} (\mathbf{x} - \mathbf{m}_{f,k}^i)}, \quad (56)$$

which measures the distance of the agents to the means of the intensities. As the swarm evolved, this distance determined which units belong to a given component. Agents were controlled according to their placement in each intensity through an open loop method using the ILQR or MPC control input obtained for each intensity. Although an open loop method was used, feedback control can be used if the state estimates are determined from the PHD filter.

The great advantage of using MPC is that the algorithm can handle nonlinearities in the objective function. Unfortunately, numerically solving an optimization at each time-step is not particularly fast, so it can be difficult to run optimization problems in real-time to control swarm robots towards a target state. This is discussed in comparison to ILQR in the Results section.

VII. Dynamical Models

To show viability of optimal swarm control via RFS, an acceleration model and a relative motion model are used to describe rover and satellite dynamics respectively. The dynamic equations of individual agents are used here to describe the dynamics of the Gaussian mixture components (means) given by the control objective Eqs. (27) and (28).

A. Acceleration Model

On a 2D plane, the linear time-invariant (LTI) system of each agent can be described by the continuous state and control matrices

$$A_c = \begin{bmatrix} 0 & 0 & 1 & 0 \\ 0 & 0 & 0 & 1 \\ 0 & 0 & 0 & 0 \\ 0 & 0 & 0 & 0 \end{bmatrix}, \quad B_c = \begin{bmatrix} 0 & 0 \\ 0 & 0 \\ 1 & 0 \\ 0 & 1 \end{bmatrix}, \quad (57)$$

and a state vector $\mathbf{x} = [x, y, \dot{x}, \dot{y}]^T$. Both x and y are defined to be the 2D positions of the agent respectively. The A_c and B_c matrices are discretized along a fixed time interval utilizing a zero-order hold assumption for the control (i.e. control is held constant over the time-interval). This results in discretized A and B matrices for the state-space equation,

$$\mathbf{x}_{k+1} = A\mathbf{x}_k + B\mathbf{u}_k. \quad (58)$$

B. Relative Motion using Clohessy-Wiltshire Equations

For a spacecraft in low Earth orbit, the relative dynamics of each spacecraft (agent), to a chief spacecraft in circular orbit, is given by the Clohessy-Wiltshire equations [41]

$$\ddot{x} = 3n^2x + 2n\dot{y} + a_x, \quad (59a)$$

$$\ddot{y} = -2n\dot{x} + a_y, \quad (59b)$$

$$\ddot{z} = -n^2z + a_z, \quad (59c)$$

where x , y , and z are the relative positions in the orbital local-vertical local-horizontal (LVLH) frame and a_x , a_y , and a_z are the accelerations in each axis respectively. The variable n is defined as the orbital frequency given by

$$n = \sqrt{\frac{\mu}{a^3}}, \quad (60)$$

where μ is the standard gravitational parameter and a is the radius of the circular orbit. The continuous state-space representation is given by

$$A_c = \begin{bmatrix} 0 & 0 & 0 & 1 & 0 & 0 \\ 0 & 0 & 0 & 0 & 1 & 0 \\ 0 & 0 & 0 & 0 & 0 & 1 \\ 3n^2 & 0 & 0 & 0 & 2n & 0 \\ 0 & 0 & 0 & -2n & 0 & 0 \\ 0 & 0 & -n^2 & 0 & 0 & 0 \end{bmatrix}, \quad B_c = \begin{bmatrix} 0 & 0 & 0 \\ 0 & 0 & 0 \\ 0 & 0 & 0 \\ 1 & 0 & 0 \\ 0 & 1 & 0 \\ 0 & 0 & 1 \end{bmatrix}, \quad (61)$$

with a state vector $\mathbf{x} = [x, y, z, \dot{x}, \dot{y}, \dot{z}]^T$ and a control input $\mathbf{u} = [a_x, a_y, a_z]^T$. These equations are discretized similarly to the acceleration model discussed previously.

VIII. Results

Using the acceleration model, which was discretized from Eq. (57) to Eq. (58), a 4-intensity swarm on a 2-D plane was initialized in a square grid where the intensities 1, 2, 3, and 4 were defined counterclockwise starting on the first quadrant. With the 4-intensity swarm, three different test cases were implemented to bring the intensities to the target trajectories and to test the control theory involved from the control formulation. The first test case compared the L_2^2 distance with varying initial conditions in a square grid with the L_2^2 quadratic distance with four target destinations

located at $(\pm 1, \pm 1)$ using MPC control. A L_2^2 plus quadratic distance comparison is also done using ILQR. The last two cases compared MPC and ILQR using the L_2^2 distance with a quadratic term and varying target destinations. For Case 2, three target destinations are located at $(\pm 1, 1)$ and $(-1, -1)$. Lastly, in Case 3, five target destinations are located at $(\pm 1, \pm 1)$ and $(0, 0)$.

Using the results of the acceleration model, control using RFS was also expanded to satellite relative motion using the Clohessy-Wiltshire Equations. Specifically, the L_2^2 plus quadratic distance was used for spacecraft formation flight. A 77-intensity swarm was initialized uniformly random between -1 and 1 on a 2D plane. Assuming that the spacecraft swarm is at lower Earth orbit, the goal for the spacecraft is to track a rotating star pattern moving counterclockwise at an orbital frequency of n .

A. Acceleration Model

1. Case 1: L_2^2 vs. L_2^2 +Quadratic Term, Four Target Destinations

For Case 1, four swarm intensities were controlled to move towards the target destinations at initial conditions farther away (square grid at $(\pm 3, \pm 3)$) and closer to (square grid at $(\pm 1.5, \pm 1.5)$) the target destinations as shown by mean responses given by the black-dashed and red-dotted lines in Figure 2(b) respectively. From the trajectory snapshots given by Figure 2(a1), initial conditions that are far from the target destinations do not have a converging control solution. From the surface visualization in Figure 1(b), the general plane is flat in areas away from the target destinations and states of the intensity. Therefore, optimization using MPC is more difficult in these flat areas and may not converge to a solution. If the intensities are initialized much closer to the target destinations as shown in Figure 2(a2), the flatness in the general plane is minimal, and the optimization step in MPC converges to a solution. By using the L_2^2 distance, converging control solutions can only be found for initial conditions and target destinations that are close.

For the L_2^2 plus quadratic distance, four swarm intensities move towards the four target destinations given by the blue-solid lines (mean responses) in Figure 2(b). Figure 2(c) shows the trajectory snapshots and final states of each of the swarm intensities during the simulation. The target destinations are plotted as black x's. The red dots are the individual swarm agents that form the Gaussian mixture intensities. From the figure, all four intensities converge to the target destinations in approximately 0.17 seconds and approximately 0.03 of steady-state error between the intensities' position to the target destinations. In comparison to only the L_2^2 distance, Figure 2(b) shows that for small distances between the initial state and the target destination, the L_2^2 distance is sufficient for state convergence, but as the distance increases, the L_2^2 distance diverges away. By adding the quadratic term to L_2^2 , the optimization step can directly determine the minimum for the control solution shown in Figure 1(c). Therefore, the target destinations attract the swarm intensities at distances that fail for only L_2^2 distance given by Figure 2(b).

The L_2^2 plus quadratic distance was also compared to ILQR. Figure 3(a) shows the trajectory snapshots and final states of the simulation. All four intensities converge to the target destinations in approximately 0.03 seconds and

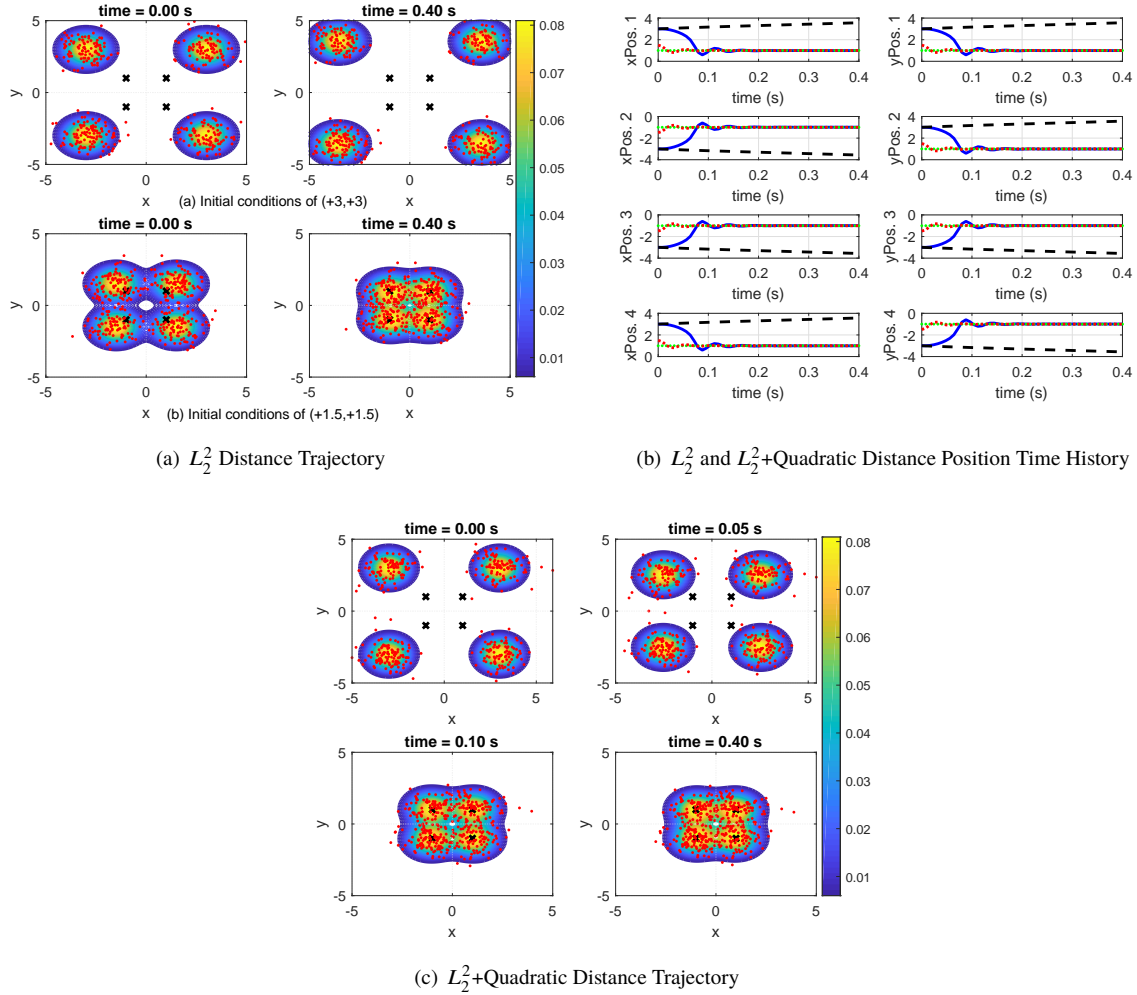


Fig. 2 Case 1: 2(a) and 2(c) show the controlled trajectories using the acceleration model and MPC. 2(b) shows the intensity mean responses from the trajectories.

approximately 0.01 of steady-state error as shown in Figure 3(b). In this figure, the x responses, y responses, and target destinations are given by blue, green, and red lines respectively. Compared to MPC, the performance significantly improved. This is because ILQR uses the full simulation horizon to calculate control inputs at each time-step. For the MPC cases, 3 time-steps in the future were used to produce the receding horizon solution. Even for three time-steps, MPC took 86.35 seconds to run while ILQR only took 2.26 seconds. Thus, ILQR's approximation of the objective function provided faster computational results even though a full-time horizon was used.

2. Case 2: Three Target Destinations

Case 2 illustrates the effect of three target destinations on the final trajectories of the four swarm intensities using MPC and ILQR.

Using MPC, the swarm intensities converged as given by the position time-history in Figure 4(b). The trajectories

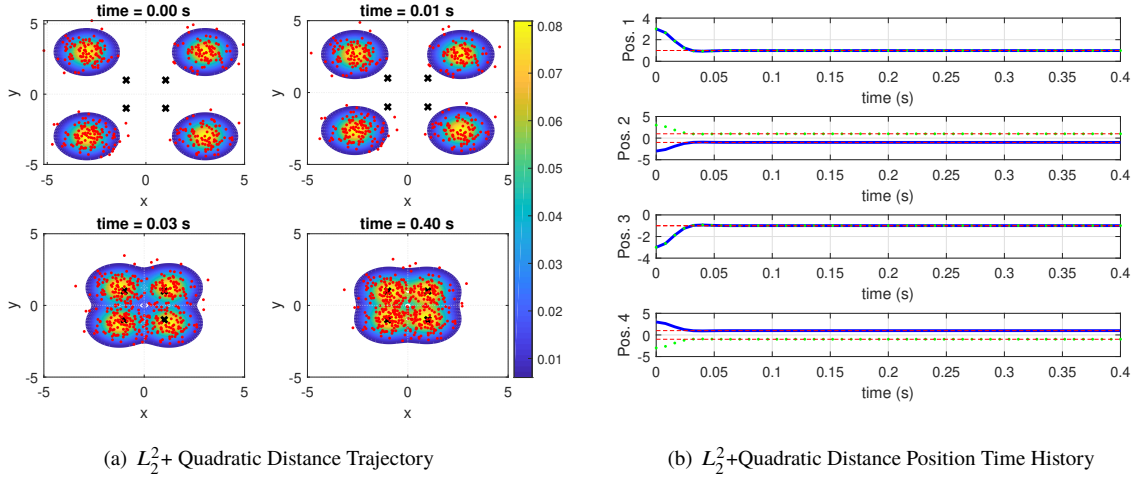


Fig. 3 Case 1: 4-intensity swarm controlled to four target destinations via ILQR. 3(a) shows the trajectories for the swarm and 3(b) shows the position time history.

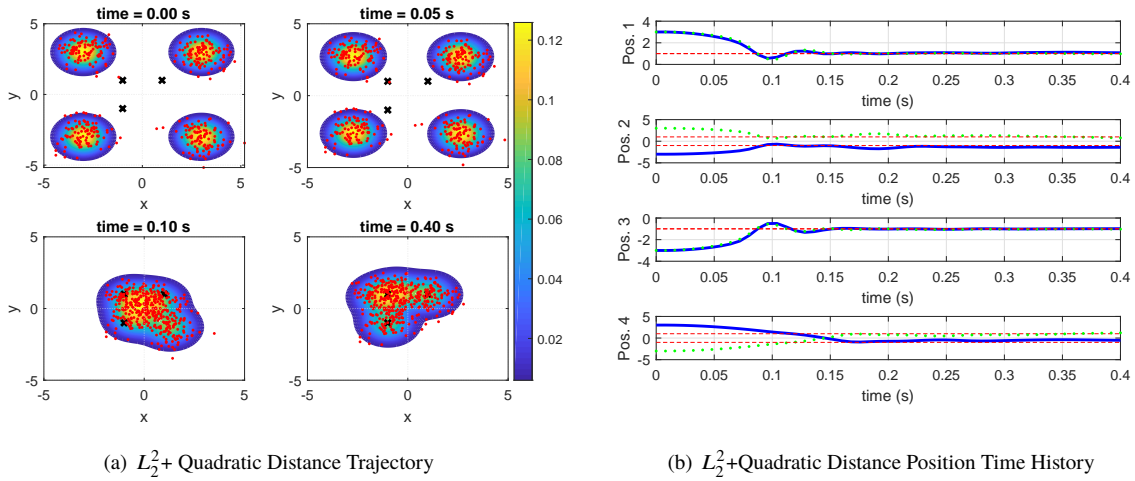


Fig. 4 Case 2: 4-intensity swarm controlled to three target destinations via MPC. 4(a) shows the trajectories for the swarm and 4(b) shows the position time history.

for intensity 1 and intensity 3 reach their target, but intensities 2 and 4 reach the third target with approximately 0.42 and 0.50 of steady-state error with 0.20 and 0.16 seconds of settling time respectively. From Figure 4(a), it can be visually shown where the swarm intensities are located relative to the target destinations at each time step. The results obtained follow directly from the RFS control theory using the L_2^2 plus quadratic distance term. By using this L_2^2 with a quadratic term in the objective function, the individual intensities will attract towards the target destinations while repulsing away from each other. This can be seen in the surface map shown in Figure 1(c), where the hills are areas of repulsion and valleys, are areas of attraction. Thus, for MPC, intensities 2 and four are attracted to the same target, but they stay away from each other which causes both to share the same target at a distance away.

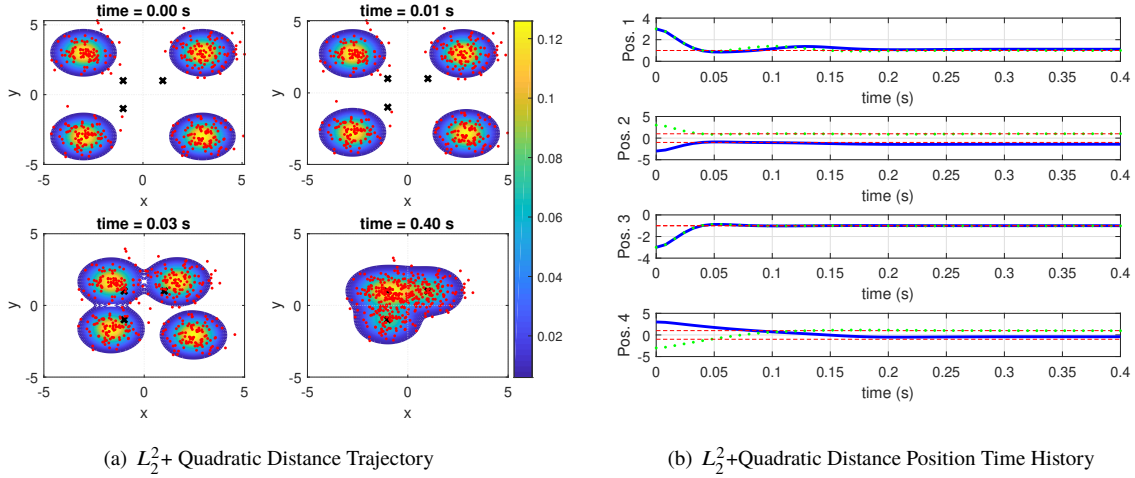


Fig. 5 Case 2: 4-intensity swarm controlled to three target destinations via ILQR. 5(a) shows the trajectories for the swarm and 5(b) shows the position time history.

This case also was compared to ILQR results. Figures 5(a) and 5(b) show the trajectory snapshots and time-history of the same swarm using ILQR. As discussed previously, due to the approximation of the objective function, the intensities 2 and 4 converged in 0.03 and 0.15 seconds with approximately 0.01 and 0.42 of steady-state error. The response was much less oscillatory than its MPC counterpart. By using the full time horizon, the ILQR was able to converge accurately rather than using a finite prediction horizon. By comparing the time-histories in Figure 5(b) and 4(b), the fourth intensity using ILQR followed very similarly to the MPC method. Therefore, there was a degree of accuracy in the approximation of the objective function to minimize for ILQR that allowed the attraction of individual intensities to the target destinations while repulsing away from each other. By providing a degree of accuracy to the objective function models given by Figure 1(c), the ILQR approximation provided computational speed to control the swarm to the target destinations.

3. Case 3: Five Target Destinations

Case 3 shows the effect of five target destinations with the four swarm intensities using MPC and ILQR. Figure 6(b) shows the time histories for all the intensities using MPC. The trajectory snapshots of the intensities are visually shown relative to the five target destinations in Figure 6(a). From Figure 6(b), all intensities converged in 0.19 seconds with a steady state error of approximately 0.17 which follow the theory as expected. Since the swarm intensities are far from each other, the effects of repulsion are minimal. Also, the intensities are attracted to the four target destinations that make up a square, but they are also attracted to the target destination at the origin. This is due to the minimization of the objective function that has a L_2^2 and a quadratic term where the individual intensities will attract towards the target destinations. Since there is an additional target destination of attraction at the origin, all four swarm intensities

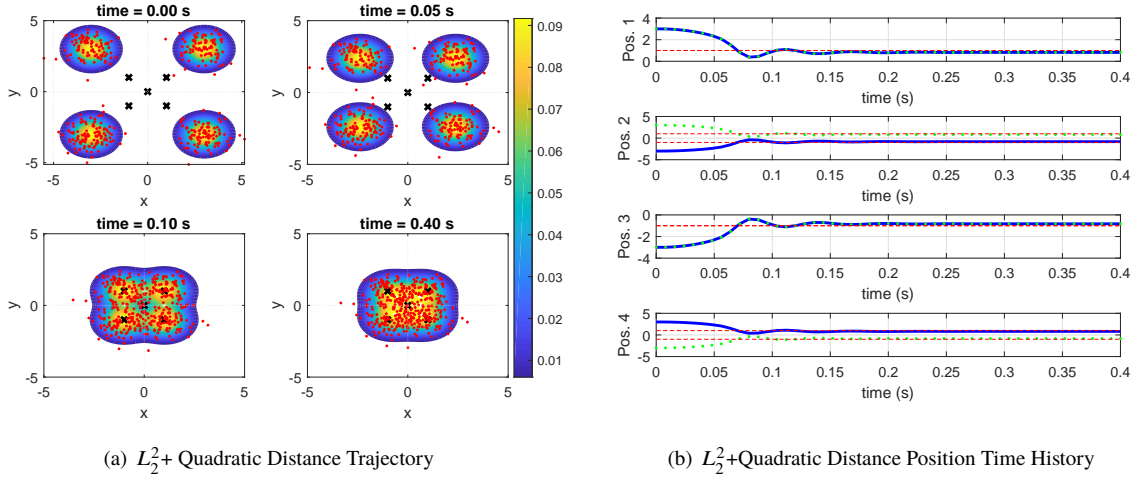


Fig. 6 Case 3: 4-intensity swarm controlled to five target destinations via MPC. 6(a) shows the trajectories for the swarm and 6(b) shows the position time history.

are affected by the origin as they are moving towards the 4 square target destinations. Thus, compared to Case 1 with only four target destinations, the intensities, in this case, will have a steady-state error due to the attraction of the target destination that has no intensity.

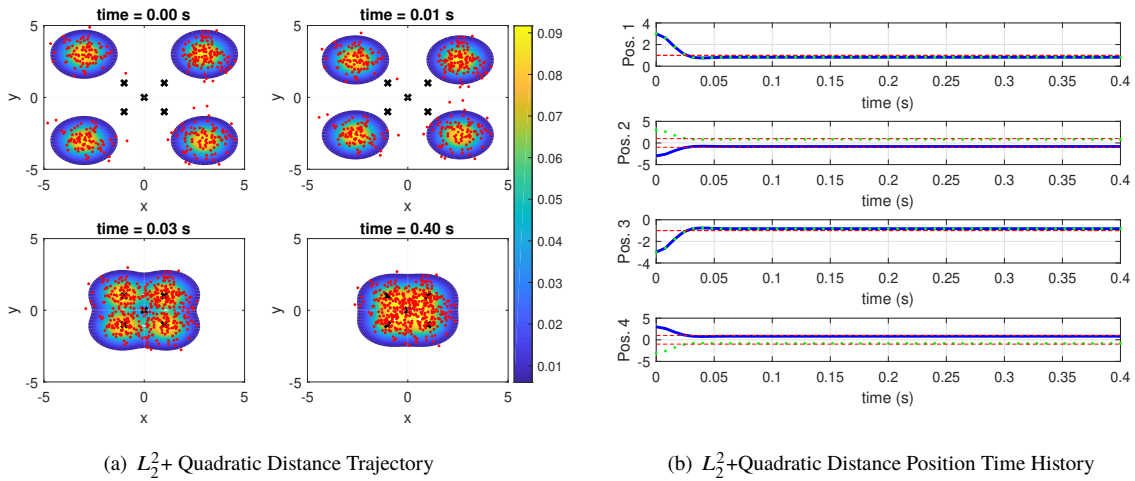


Fig. 7 Case 3: 4-intensity swarm controlled to five target destinations via ILQR. 7(a) shows the trajectories for the swarm and 7(b) shows the position time history.

ILQR was also used to compare how five target destinations affected the quadratization of the L_2^2 plus quadratic objective function. Figures 7(a) and 7(b) show the trajectory snapshots and time-history respectively. The swarm converged in 0.03 seconds and 0.12 of steady-state error. This steady-state error shows the attraction of the target destination at the origin which follows directly from results from the L_2^2 plus quadratic distance given by Figure 1(c). Similar to Case 1 and Case 2, ILQR only takes 2.43 seconds for a full horizon control trajectory while MPC takes 102.02

seconds to simulate the whole trajectory using a prediction horizon of 3 time-steps. Therefore, ILQR is the method of choice to get better performance characteristics (using the full horizon) for much less computational time than MPC.

B. Clohessy-Wiltshire Relative Motion

1. Relative Motion with Perfect Information

For the spacecraft relative motion, 77 intensities were birthed at the initial time from uniformly random initial conditions between -1 and 1 m from the chief satellite in a circular orbit. The goal was to control the spacecraft into a moving star-shaped pattern. Both the spacecraft and the rotating star pattern had an orbital frequency of $n = 0.00110678$ rad/s. It was assumed that the information received throughout the simulation was perfect. Figure 8(a) shows the trajectory snapshots of the spacecraft (contours) and the target destinations (black x's) using ILQR and the L_2^2 plus quadratic distance. The intensities, represented by each contour, can be safely assumed to contain a single agent. As time progresses, the swarm intensities converge quickly into the formation and maintain the formation for the simulation time of 40 s. Figure 8(b) shows the acceleration for five spacecraft intensities to stay in the star formation. From these results, control using RFS can be expanded to physical spacecraft systems and can be used for moving targets.

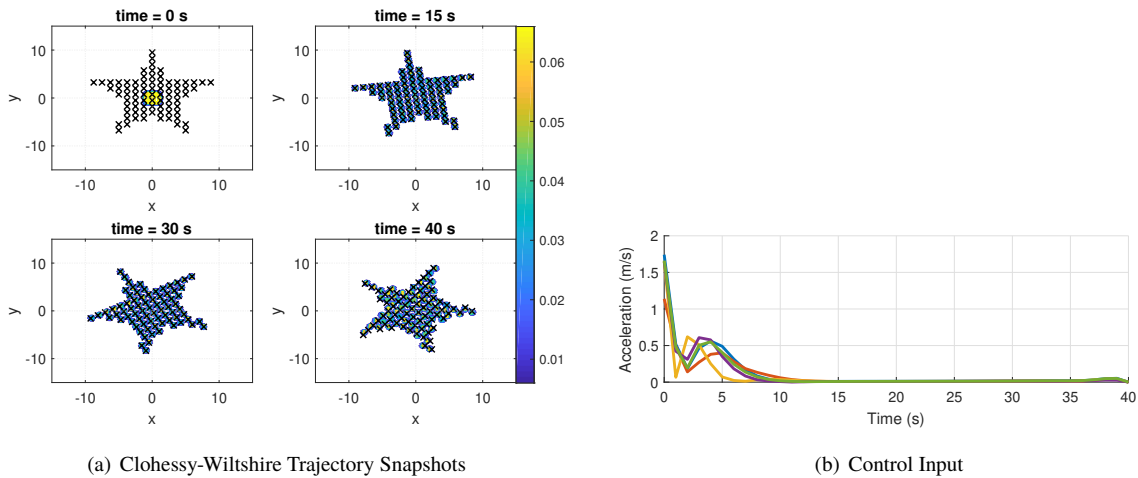


Fig. 8 77-intensity spacecraft swarm controlled to a rotating star target via ILQR with perfect information. 8(a) shows the trajectories and 8(b) shows the acceleration for five spacecraft intensities.

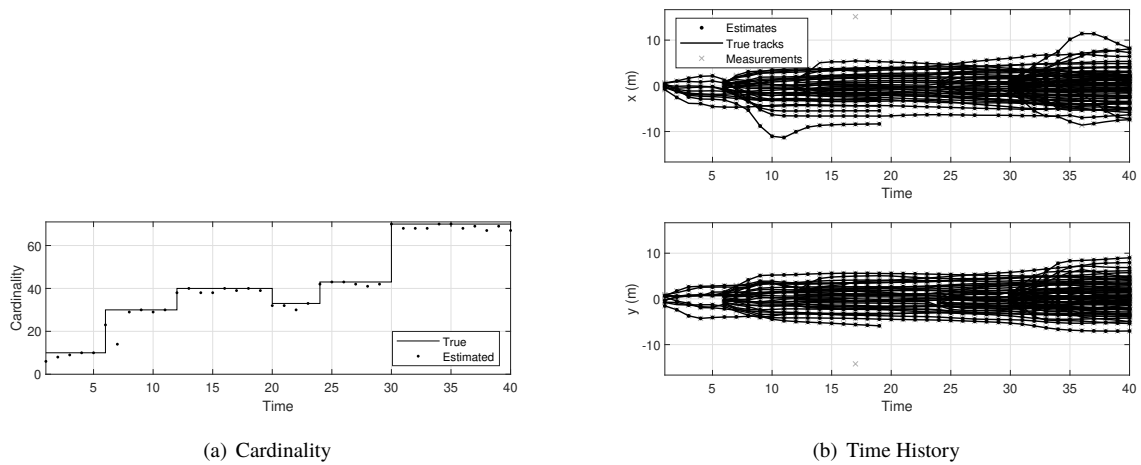
2. Relative Motion with Imperfect Information

Next, the imperfect information (i.e. process, measurement, and clutter noise) was included in the simulation. In order to control with imperfect information, the GM-PHD filter was used in a feedback loop with the RFS control method. The GM-PHD filter would determine the estimates of the intensities which would be used for RFS control. The problem was altered to be more complicated by including differing birth and death times for the agents. With the addition of imperfect information and complication of changing number of agents, using the GM-PHD filter provides

accurate estimates of the agents through time which allows for RFS control in the loop. Figure 9(a) shows the cardinality or number of agents in the swarm through time. The solid line is the true number of agents while the dotted line shows the estimate at each time-step. At each time-step, the agent estimates were fed through the RFS control using ILQR to obtain a control input for each agent. Then, the estimates were controlled and fed back to the GM-PHD filter at the next time-step. Figure 9(c) shows the snapshots of the controlled agents (black circles) and targets (green stars) at each time-step. Figure 9(b) shows the time history for the true agents (solid lines), estimated agents (black dots), and overall measurements (gray x's). From Figure 9(a), as the true agents die or birth initially, estimates of the occurrence is accurate. As the number of agents increases, the estimates become less accurate. This is because the GM-PHD filter only uses the first-order statistical moment to propagate the cardinality information of agents [42]. The cardinality distribution is unknown, and it is approximated as a Poisson distribution. For a Poisson distribution, the mean and covariance are equal. Therefore, if there are a larger number of agents in the field, the corresponding covariance of the cardinality distribution is also higher. Although the estimates are less accurate, the individual agents are controlled successfully into a star pattern in the presence of imperfect information. This is shown directly in 9(c) and 9(b). As agents die or birth, the control input dies, or births with it, and due to the L_2^2 plus quadratic distance, agents are flexible to move into different parts of the formation.

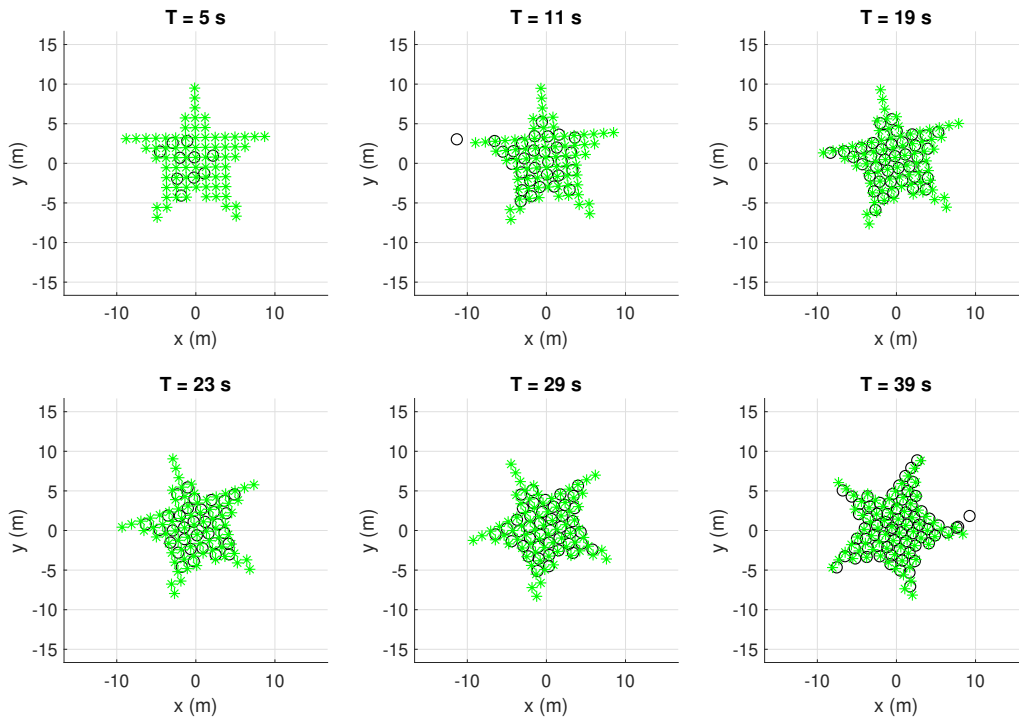
IX. Conclusions

The objective of this paper is to formulate a method to control swarming formations using MPC and ILQR from RFS theory. By setting up the problem using information divergence to define the distance between the swarm RFS and the desired distribution, an optimal control problem is found that tracks a linear system with a nonquadratic objective function using MPC and ILQR that approximates the optimal control solution which minimizes the objective function. It is shown that by formulating the objective function that uses a L_2^2 distance only, the intensities converge only at close proximity to the target destinations as shown in Case 1. By adding the quadratic term, the trajectories of the intensities converge to the target destinations at distances where L_2^2 distance fails. By using ILQR for Case 1, the trajectories are found in a more computationally efficient manner compared to MPC. The MPC optimization is solved at three time-step intervals for the nonquadratic objective function which becomes computationally complex. ILQR is computed using the full-time horizon, and it still evaluates in a lot less time than MPC. Cases 2 and 3 show the repulsion of individual intensities to each other and the attraction of each intensity to the target destinations respectively using MPC and ILQR. Thus, the number of destination states do not have to be the same number of swarm intensities for the controller to work, and the approach can be adaptive to swarm size. The RFS control formulation via MPC or ILQR takes the number of destinations into account during the optimization of the solution. Again, ILQR exceeds MPC in computational efficiency due to an approximation of the nonlinear dynamics and nonquadratic cost functions. Lastly, control using RFS is also applied to the spacecraft relative motion problem with perfect and imperfect information. In the simulation with perfect



(a) Cardinality

(b) Time History



(c) Clohessy-Wiltshire Trajectory Snapshots

Fig. 9 77-agent spacecraft swarm controlled to a rotating star target via ILQR with imperfect information. 9(a) shows the true and estimated cardinality, 9(b) shows the time history of the true tracks, the estimated tracks, and overall measurements, and 9(c) shows the trajectories for the spacecraft agents and targets.

information, control via RFS still provides a converging control solution with a large number of Gaussian mixtures and rotating targets. For the imperfect information case, the GM-PHD filter can achieve accurate estimates to allow for a converging RFS control solution of variable swarm size. These examples show the benefit of control using RFS by overcoming the curse of dimensionality.

ACKNOWLEDGMENT

The authors wish to acknowledge support by the National Aeronautics and Space Administration under Contract Number NNX16CP45P issued through the NASA STTR Program by the Jet Propulsion Laboratory (JPL) and led by Amir Rahmani at JPL. The authors wish to acknowledge useful conversations related to satellite technologies with Chuck Hisamoto, Vaughn Weirens, and Suneel Sheikh of ASTER Labs, Inc. The authors wish to acknowledge Andrew Akerson, a graduate student at the California Institute of Technology, who enabled useful notation for the mathematical theory used in the paper. Lastly, the authors wish to acknowledge Piyush M. Mehta, Assistant Professor at West Virginia University, for providing useful conversations in structuring and optimizing code.

References

- [1] Kube, C. Ronald, and Hong Zhang. "Collective robotics: From social insects to robots." *Adaptive behavior* 2.2 (1993): 189-218.
- [2] Vassev, Emil, Mike Hinchey, and Joey Paquet. "Towards an ASSL specification model for NASA swarm-based exploration missions." *Proceedings of the 2008 ACM symposium on Applied computing*. ACM, 2008.
- [3] Ryan, Allison, et al. "An overview of emerging results in cooperative UAV control." *Decision and Control, 2004. CDC. 43rd IEEE Conference on*. Vol. 1. IEEE, 2004.
- [4] Rubenstein, Michael, Alejandro Cornejo, and Radhika Nagpal. "Programmable self-assembly in a thousand-robot swarm." *Science* 345.6198 (2014): 795-799.
- [5] Lunze, Jan. *Feedback control of large-scale systems*. London: Prentice-Hall, (1992): 9-11.
- [6] Foderaro, Greg, Silvia Ferrari, and Thomas A. Wettergren. "Distributed optimal control for multi-agent trajectory optimization." *Automatica* 50.1 (2014): 149-154.
- [7] Rudd, Keith, Greg Foderaro, and Silvia Ferrari. "A generalized reduced gradient method for the optimal control of multiscale dynamical systems." *Decision and Control (CDC), 2013 IEEE 52nd Annual Conference on*. IEEE, 2013.
- [8] Foderaro, Greg, et al. "Distributed optimal control of sensor networks for dynamic target tracking." *IEEE Transactions on Control of Network Systems* (2016).
- [9] Ferrari, Silvia, et al. "Distributed optimal control of multiscale dynamical systems: a tutorial." *IEEE Control Systems* 36.2 (2016): 102-116.
- [10] Huang, Minyi, Roland P. Malhamé, and Peter E. Caines. "Large population stochastic dynamic games: closed-loop McKean-Vlasov systems and the Nash certainty equivalence principle." *Communications in Information & Systems* 6.3 (2006): 221-252.
- [11] Pace, M., M. Birattari, and M. Dorigo. "The swarm/potential model: Modeling robotics swarms with measure-valued recursions associated to random finite sets." *IEEE Transactions on Robotics*, page submitted (2013).

- [12] Centralized Control. Ian Sommerville , 2008. Web. 05 May 2017.
- [13] Mondada, Francesco, et al. "The cooperation of swarm-bots: Physical interactions in collective robotics." *IEEE Robotics & Automation Magazine* 12.2 (2005): 21-28.
- [14] Bandyopadhyay, Saptarshi, Soon-Jo Chung, and Fred Y. Hadaegh. "Probabilistic swarm guidance using optimal transport." *Control Applications (CCA), 2014 IEEE Conference on.* IEEE, 2014.
- [15] Acikmese, Behçet, and David S. Bayard. "A markov chain approach to probabilistic swarm guidance." *American Control Conference (ACC), 2012.* IEEE, 2012.
- [16] Reif, John H., and Hongyan Wang. "Social potential fields: A distributed behavioral control for autonomous robots." *Robotics and Autonomous Systems* 27.3 (1999): 171-194.
- [17] Chattopadhyay, Ishanu, and Asok Ray. "Supervised self-organization of homogeneous swarms using ergodic projections of markov chains." *IEEE Transactions on Systems, Man, and Cybernetics, Part B (Cybernetics)* 39.6 (2009): 1505-1515.
- [18] Bandyopadhyay, Saptarshi, Soon-Jo Chung, and Fred Y. Hadaegh. "Inhomogeneous Markov chain approach to probabilistic swarm guidance algorithm." *5th Int. Conf. Spacecraft Formation Flying Missions and Technologies.* 2013.
- [19] Hadaegh, Fred Y., Soon-Jo Chung, and Harish M. Manohara. "On development of 100-gram-class spacecraft for swarm applications." *IEEE Systems Journal* 10.2 (2016): 673-684.
- [20] Eren, Utku, and Behçet Açıkmeşe. "Velocity field generation for density control of swarms using heat equation and smoothing kernels." *IFAC-PapersOnLine* 50.1 (2017): 9405-9411.
- [21] Camacho, Eduardo F., and Carlos Bordons Alba. *Model predictive control.* Springer Science & Business Media, 2013.
- [22] Di Cairano, S., H. Park, and I. Kolmanovsky. "Model predictive control approach for guidance of spacecraft rendezvous and proximity maneuvering." *International Journal of Robust and Nonlinear Control* 22.12 (2012): 1398-1427.
- [23] Manikonda, V., et al. "A model predictive control-based approach for spacecraft formation keeping and attitude control." *American Control Conference, 1999. Proceedings of the 1999.* Vol. 6. IEEE, 1999.
- [24] Morgan, Daniel, Soon-Jo Chung, and Fred Y. Hadaegh. "Decentralized model predictive control of swarms of spacecraft using sequential convex programming." *Advances in the Astronautical Sciences* 148 (2013): 1-20.
- [25] Morgan, Daniel, Soon-Jo Chung, and Fred Hadaegh. "Spacecraft swarm guidance using a sequence of decentralized convex optimizations." (2012): Art-No.
- [26] Morgan, Daniel, Soon-Jo Chung, and Fred Y. Hadaegh. "Swarm assignment and trajectory optimization using variable-swarm, distributed auction assignment and model predictive control." *AIAA guidance, navigation, and control conference.* 2015.
- [27] Doerr, Bryce and Richard Linares. "Control of Large Swarms via Random Finite Set Theory." *2018 Annual American Control Conference (ACC)* (2018): 2904-2909.

- [28] Ma, Wing-Kin, et al. "Tracking an unknown time-varying number of speakers using TDOA measurements: A random finite set approach." *IEEE Transactions on Signal Processing* 54.9 (2006): 3291-3304.
- [29] Mahler, Ronald PS. "Multitarget Bayes filtering via first-order multitarget moments." *IEEE Transactions on Aerospace and Electronic systems* 39.4 (2003): 1152-1178.
- [30] Vo, B-N., and W-K. Ma. "The Gaussian mixture probability hypothesis density filter." *IEEE Transactions on signal processing* 54.11 (2006): 4091-4104.
- [31] Todorov, Emanuel, and Weiwei Li. "A generalized iterative LQG method for locally-optimal feedback control of constrained nonlinear stochastic systems." *American Control Conference, 2005. Proceedings of the 2005. IEEE, 2005.*
- [32] Hoang, Hung Gia, et al. "The Cauchy Schwarz divergence for Poisson point processes." *IEEE Transactions on Information Theory* 61.8 (2015): 4475-4485.
- [33] Banerjee, Arindam, et al. "Clustering with Bregman divergences." *Journal of machine learning research* 6.Oct (2005): 1705-1749.
- [34] Inaba, Masayuki, and Peter I. Corke. "Linear-quadratic control and smoothing." *Robotics Research: The 16th International Symposium ISRR*. Switzerland: Springer, 2016. 43-47. Print.
- [35] Bellman, Richard. "The theory of dynamic programming." *Bulletin of the American Mathematical Society* 60.6 (1954): 503-515.
- [36] Tassa, Yuval, Nicolas Mansard, and Emo Todorov. "Control-limited differential dynamic programming." *Robotics and Automation (ICRA), 2014 IEEE International Conference on. IEEE, 2014.*
- [37] Liao, Li-zhi, and Christine A. Shoemaker. "Advantages of differential dynamic programming over Newton's method for discrete-time optimal control problems." *Cornell University, 1992.*
- [38] Liao, L-Z., and Christine A. Shoemaker. "Convergence in unconstrained discrete-time differential dynamic programming." *IEEE Transactions on Automatic Control* 36.6 (1991): 692-706.
- [39] Findeisen, Rolf, and Frank Allgöwer. "An introduction to nonlinear model predictive control." *21st Benelux Meeting on Systems and Control*. Vol. 11. Eindhoven, The Netherlands: Technische Universiteit Eindhoven Veldhoven, 2002.
- [40] Find minimum of unconstrained multivariable function - MATLAB fminunc, MathWorks. Web.
- [41] Curtis, Howard D. *Orbital mechanics for engineering students*. Butterworth-Heinemann, 2013.
- [42] Mahler, Ronald. "PHD filters of higher order in target number." *IEEE Transactions on Aerospace and Electronic systems* 43.4 (2007).